JGR Planets

RESEARCH ARTICLE
10.1029/2023JE008039

Geologic History of Deuteronilus Cavus in the Ismenius Lacus Region, Mars

Lukas Wueller[1], Wajiha Iqbal[1], Harald Hiesinger[1], and James W. Head III[2]

[1]Institut für Planetologie, Universität Münster, Münster, Germany, [2]Department of Earth, Environmental, and Planetary Sciences, Brown University, Providence, RI, USA

Key Points:

- We have produced the first high-resolution map of Deuteronilus Cavus in the fretted terrain south of the Martian dichotomy boundary
- The region records a complex erosional and depositional history, including fluvial and glacial processes in the Amazonian period
- This study provides a framework for exploration of high-obliquity mid-latitude plateau glaciation

Correspondence to:
L. Wueller,
lwueller@uni-muenster.de

Citation:
Wueller, L., Iqbal, W., Hiesinger, H., & Head, J. W., III (2024). Geologic history of Deuteronilus Cavus in the Ismenius Lacus region, Mars. *Journal of Geophysical Research: Planets*, *129*, e2023JE008039. https://doi.org/10.1029/2023JE008039

Received 3 AUG 2023
Accepted 16 JAN 2024

Abstract The Ismenius Lacus region of Mars has a diverse geological history, and we present the first high-resolution map of Deuteronilus Cavus (36.2°N; 14.0°E, ∼120 km diameter) in the fretted terrain south of the dichotomy boundary. Strong evidence suggests a volcanic origin of the regional plains, based on the ∼50 m thick volcanic bed underlying 180–300 m of sublimation residue associated with Amazonian plateau glaciation. Pervasive external volcanic flooding, internal erosional modification, and enlargement of a pre-existing crater by up to 175%–200% resulted in the cavus' present shape. The phyllosilicates detected within Deuteronilus Cavus could be primary materials associated with the surficial aqueous activity, subsurface alteration products excavated by impacts, or a combination of both. We observe branching fluvial channels that are more recent than the traditional valley networks and may be related to fretted terrain resurfacing during the waning period of a high-obliquity glaciation phase. This is consistent with our interpretation of the ∼600 m thick lobate and lineated deposits, which are remnants of receding glaciers. The glacial ice, protected by a 15–20 m insulating layer of debris cover, is of significant interest for future landing missions because of its potential to preserve biological and climatological signatures, to provide a critical test of Amazonian plateau glaciation, and to be used for in situ resource utilization. With our detailed geological mapping, we improved our understanding of the geological evolution and climatic conditions in the enigmatic fretted terrain near the dichotomy boundary.

Plain Language Summary The ∼120 km long Deuteronilus Cavus was initiated by an impact event. The resulting impact crater was modified by glacial erosional and fluvial processes, leading to the enlargement of 175%–200% of the pre-existing crater. In addition, we find strong evidence for recent glaciation (<1 Ga) that left 180–300 m of sublimation residue on the plateau superimposed on a ∼50 m thick volcanic bed, suggesting a volcanic origin of the regional plains. During the waning period of a high-glacial phase, the meltwater ponded on the surface of the cavus, altered surface rocks to produce phyllosilicates, formed channels (now observed as inverted sinuous ridges), and locally distributed branched fluvial channels that are more recent than the traditional valley networks. Glacial landforms still contain up to 600 m of remnant ice from the retreating glaciers at the end of the last glacial period. The relatively pure ice, protected by a 15–20 m insulating layer of debris cover, is critical for future landing missions because of its potential to preserve biological and climatological signatures and to be used for in situ resource utilization. Overall, this research enhances our understanding of the geological evolution and climatic history of Mars.

1. Introduction

Geological units of the Ismenius Lacus quadrangle (MC-5, Lucchitta, 1977, 1978) span large parts of Martian history, ranging from Noachian-aged highlands and plateaus to Amazonian-aged deposits (Baker & Head, 2015; Tanaka et al., 2014). The quadrangle contains the regions of the Arabia Terra bench (Protonilus Mensae) and Deuteronilus Mensae (DM) and hosts a variety of morphologies and landforms, which are commonly associated with glacial (Head et al., 2005; van Gasselt et al., 2011), periglacial (van Gasselt et al., 2011), and paraglacial (Jawin & Head, 2021; Jawin et al., 2018) environments. Viscous flow of ice-rich materials, that is, lobate debris aprons (LDA) and lineated valley fill (LVF), record midlatitude glaciation and mantling during the Middle Amazonian period (Baker & Head, 2015; Morgan et al., 2009). Obliquity-forced cycles of ice deposition and accumulation lead to variations in morphology, distribution, and behavior of glacial-related landforms due to changing surface and subsurface water-ice stability (Carr & Head, 2010; Neukum et al., 2004).

Our geologically complex mapping area (Figures 1–4) includes the ∼120 km Deuteronilus Cavus centered at 36.2°N; 14.0°E, branching channels suggesting fluvial and glacial activity, possibly witnessing changing climate

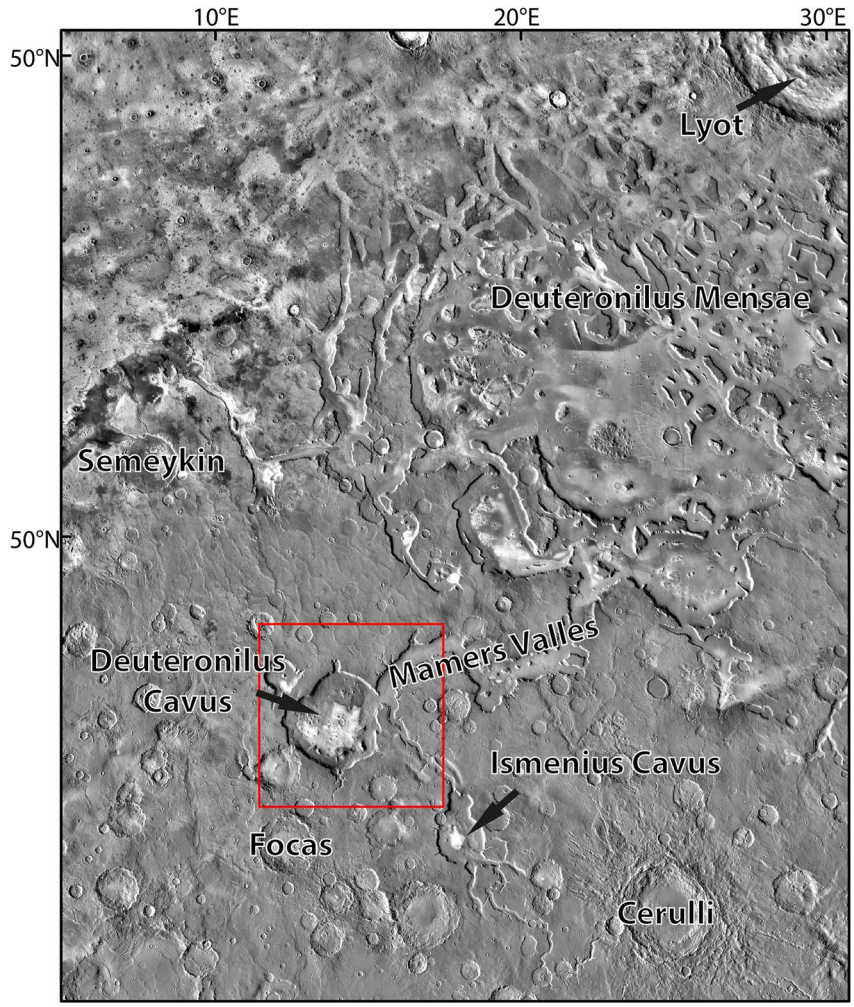

Figure 1. Regional context of our mapped area (red box shows the extent of Figure 2) in the fretted terrain south of the dichotomy boundary on a THEMIS-IR daytime basemap. The area shown is within the Ismenius Lacus quadrangle MC-05 (Batson et al., 1979).

conditions, evidence for phyllosilicates, wrinkle ridges on degraded plateaus, and various deposits of different morphologies and textures. To the southeast of the mapping region lies the depression of Ismenius Cavus, which is considered to be an important exploration zone and landing region for future Mars missions due to its ancient lake deposits and clay minerals surrounded by Amazonian glaciers (Dehouck et al., 2010). Our current study region provides similar exploration opportunities, but offers a more diverse geology as well as potentially larger volumes of resource deposits. Hence, we created a new comprehensive geologic map to provide the geologic framework for possible future in situ resource utilization (ISRU), and addressed the following scientific questions: (a) What are the stratigraphic relationships between the geologic units, and what information can we gain about the chronostratigraphy of our map area, and the climate conditions throughout Martian history? (b) What is the origin of Deuteronilus Cavus in our research area? (c) When and how were phyllosilicates formed? (d) How does the sequence and nature of our mapped units help constrain the origin of the fretted terrain (a complex combination of cliffs, mesas, buttes, and straight-walled/sinuous valleys; Sharp, 1973) and the dichotomy boundary (the major topographic division between the northern lowlands and southern uplands)? (e) What specific targets in our research area are of interest for future lander missions, and which units are suitable for studies of climatological and potential biological signatures?

2. Regional Setting and General History of Arabia Terra and the Ismenius Lacus Region

On the basis of global geological mapping of Mars (Tanaka et al., 2014) and the general framework of Mars geologic history (Carr & Head, 2010) the geologic setting of the Ismenius Lacus region consists of a basement of early Martian crustal material highly modified by Pre-Noachian and Early Noachian impact bombardment, creating the Borealis Basin in the northern lowlands (Andrews-Hanna et al., 2008), and later superposed crater and basin deposits forming the primary upland cratered terrain. As outlined by McGill (2000), the geological history of the north-central Arabia Terra region, in which Ismenius Lacus and our map area lie, consists of this cratered highland basement that formed in the Pre-Noachian and Early Noachian. The region was then extensively resurfaced by plains, likely to be of volcanic origin (McGill, 2000) in the Late Noachian, forming the regionally flat highland plateau and burying ejecta, smaller craters, and related materials that had formed in the Middle Noachian. According to McGill (2000), the emplacement of the Late Noachian regional volcanic plains was followed by the formation of the fretted terrain (Sharp, 1973), a series of stubby alcoves, sinuous channels and groups of individual flat-topped and rounded mesas that become increasingly prominent and abundant from the south to the north across Arabia Terra and that dominate the region of the dichotomy boundary.

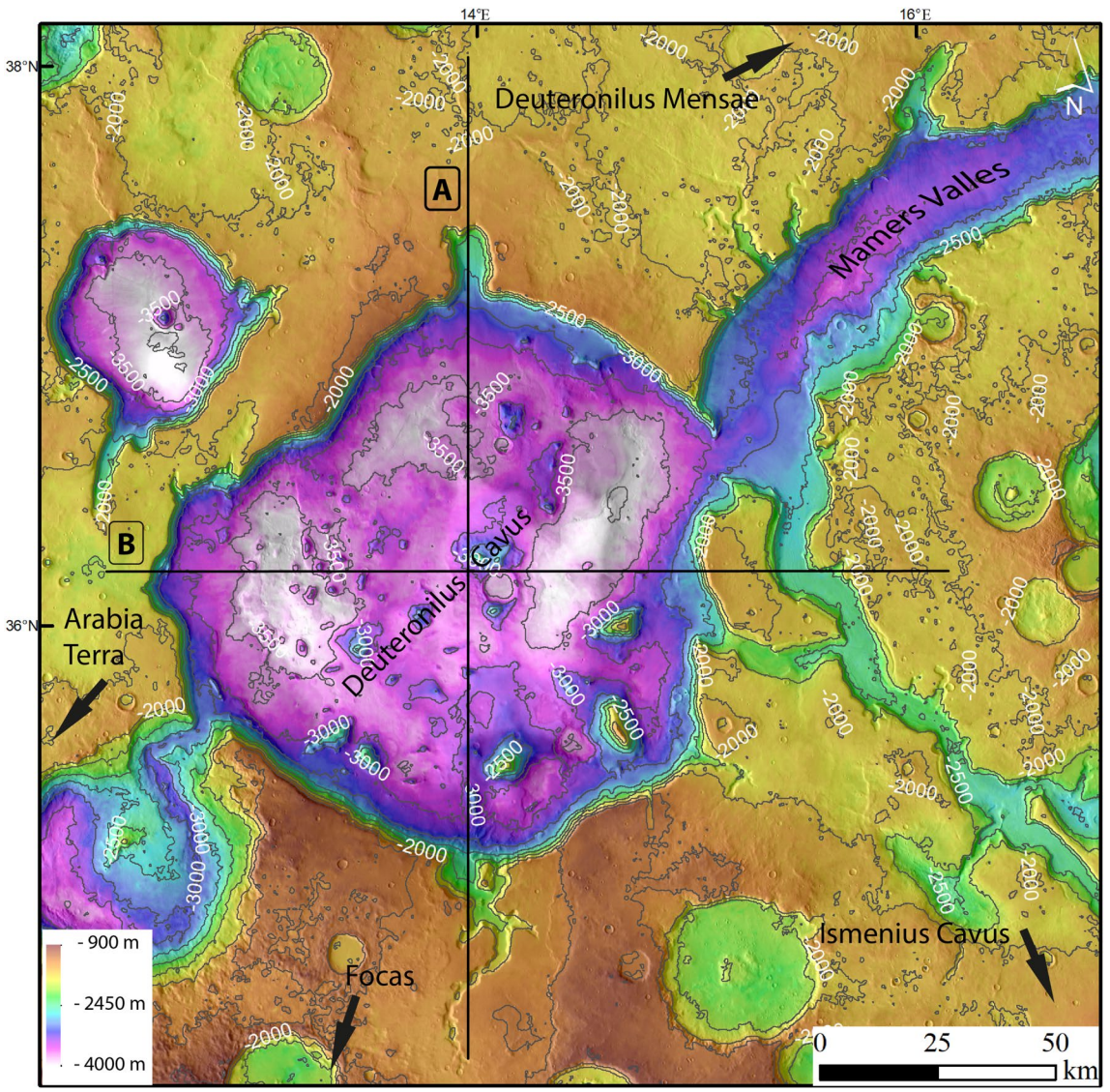

Figure 2. HRSC-MOLA Blended DEM over THEMIS-IR daytime view of the wider study area with 250 m contour lines. The black boxes and black lines show the position of the topographic profiles shown in Figure 3.

McGill (2000) interpreted the fretted terrain age as Late Noachian-Early Hesperian and provided abundant evidence that the flow of liquid water was involved in its formation. He noted the presence of local small sinuous valleys, but pointed out their differences in morphology and density in this region compared to the traditional "valley networks" (e.g., Carr, 1995; Hynek et al., 2010). He also interpreted the lobate and lineated material that currently fills many of the fretted terrain's stubby alcoves and sinuous channels to be of a much younger, Amazonian age (see McGill, 2000, Figure 15, p. 6958), and of possible debris flow/rock glacier origin. As a result, aeolian, fluvial, and glacial erosion and deposition features characterize the geomorphologic inventory of the region (Baker & Head, 2015; Head et al., 2003). Our geological map of Deuteronilus Cavus in the Ismenius Lacus quadrangle (Figure 1) builds on this foundation and addresses a series of outstanding questions concerning the nature and origin of the regional plains; the burial of pre-plains craters; the origin of cavi; the nature, timing and origin of the fretted terrain, the nature, timing and origin of the unusual "valley networks"; and the processes associated with fretted valley lobate and lineated fill and their relation to the current plateau surface deposits.

The regional altitude is relatively low with elevations below the planetary reference. Ranging from the plateaus (−900 m) to the floor of Deuteronilus Cavus (−4,000 m), the maximum altitude difference within our mapping area is ∼3,000 m. The regional topographic trend shows that the map area is tilted toward the north, showing a local altitude difference of ∼100 m over a distance of ∼190 km between the southern and the northern boundary of our research area (Figure 3a). The prominent Deuteronilus Cavus depression is located ∼1,650 m below the adjacent elevation and covers much of the mapping area. The cavus rim is not upraised and the rim topography slopes toward the cavus interior. Mamers Valles intersects Deuteronilus Cavus to the east, is ∼800 m below the surrounding plateaus (Figure 3b) and widens in the NE-direction (Figure 1).

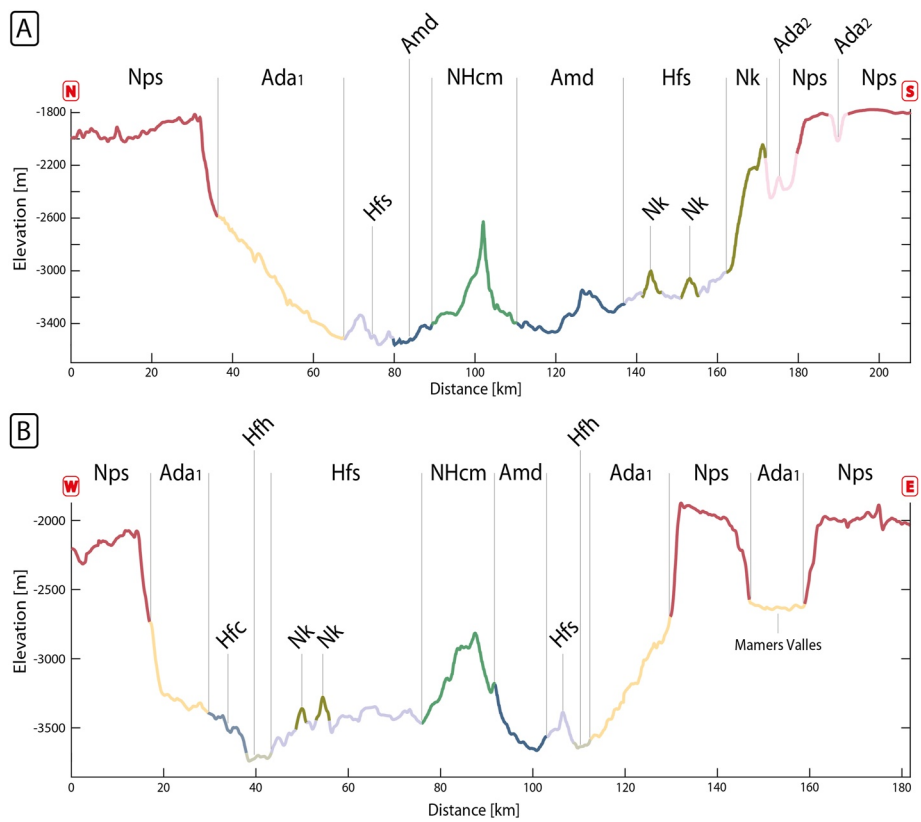

Figure 3. (a) Topographic N-S profile and (b) W-E profile (both 30x vertical exaggeration) with geological unit boundaries indicated. The geographic position of these profiles is shown in Figure 2.

3. Data Sets and Mapping Technique

To generate a higher resolution geological map, we performed mapping at a digitization scale of 1:250,000 using ESRI's ArcMap geographic information system 10.5.1. on the basis of five individual data sets: (a) THEMIS-IR daytime and (b) THEMIS-IR nighttime data with a pixel scale of ∼100 m/px (Christensen et al., 2004) provide information on the thermal emission of different surface materials; (c) CTX image data acquired by the Context Camera aboard the Mars Reconnaissance Orbiter with a pixel scale of ∼6 m/px formed the basis of our geological mapping. The CTX mosaics obtained from The Bruce Murray Laboratory for Planetary Visualization (http://murray-lab.caltech.edu/CTX/, Dickson et al., 2018) provide global coverage but are less suitable for photo-based mapping in this region as the image comparability is limited when illumination conditions change between acquisition times. For this reason, we locally complemented the mosaics with individual CTX strips of appropriate illumination; (d) HiRISE images were used where available to perform small-scale observations with a pixel scale of 0.25–1 m/px (McEwen, 2007); and (e) the HRSC-MOLA Blended DEM with a pixel scale of ∼200 m/px (Fergason et al., 2018) was used for regional topographic context and assessments. All data sets were acquired via the Multi-Temporal Database for Planetary Image Data (MUTED, Heyer et al., 2018).

Our map covers an area of approximately 28,500 km^2 extending from 34.5°N; 12.5°E to 37.7°N; 15.7°E (Figure 2) within the MC-5 quadrangle (Batson et al., 1979, Figure 1). Deuteronilus Cavus covers ∼40% of our research area. Ismenius Cavus is located ∼200 km to the southeast and Focas crater about 160 km to the southwest (distances measured from crater center to cavus center; Figure 1). For our map, we followed the standard photogeological methods of Tanaka et al. (2009). Certain contacts were mapped based on definite morphologic, structural, and stratigraphic relationships of the units using CTX, HiRISE and topographic data. In addition to these data sets, THEMIS data were used to identify transitional, less well-defined unit boundaries, which we termed approximate contacts. To maximize the comparability with previous maps of the region, the symbology used follows the standards of the Federal Geographic Data Committee (FGDC, 2006), and the nomenclature used is consistent with the Gazetteer of Planetary Nomenclature (Blue, 1999).

4. Results

We produced a comprehensive geological map of the region at a print scale of 1:1M using various data sets described above (Figure 4).

4.1. Unit Descriptions and Interpretations

4.1.1. Plateau Materials

Nps—Plateau materials—The plateau unit is one of the main units in the mapping area comprising the clear majority of the mapped region. It is regionally flat, and its topographic elevation decreases very slightly from south to north by around 100 m (Figure 3a), following the general topographic trend of the surrounding area toward the dichotomy boundary and the northern lowlands (Figure 1). Craters with diameters between 5 and 50 km are superposed on the Plateau materials and are widespread (Figure 2), some of which have pedestal ejecta (Figure 5b) or lobate ejecta (Figure 5d). Furthermore, three graben with a preferential NNE-SSW-orientation, one NW-SE-oriented sinuous rile, and several wrinkle ridges (Pauw et al., 2023, <12 km length, ∼30 m height) without a clearly preferred orientation can be discerned superposed on the Plateau materials. At large scale, outside the map area (Figure 1), many wrinkle ridges show a preferential NNW-SSE-orientation and can be up to 100 km in length (Pauw et al., 2023). Channels showing different stages of branching converge toward plateau edges and alcoves. Some crater rims have been strongly eroded, resulting in craters with barely visible rims. In some areas, fragments of the plateau unit have been tilted, broken off and moved into valleys or craters. An internal dark layer is exposed on the steep slopes of Mamers Valles and Deuteronilus Cavus. This dark layer is approximately 50 m thick (Figure 6), protrudes from the slopes, and its outcrop is rough-textured compared to the overlying materials. The plateau light surface layer varies in thickness from 180 to 200 m in the western wall of the cavi (Figure 6a) to about 260–300 m in the northern wall of Mamers Valles (Figure 6b).

Interpretation: The plateau unit is part of the surrounding highlands, is the oldest unit in the mapping area, and consists primarily of volcanic materials, impact breccia, their erosional products, and sublimation residue associated with an Amazonian plateau glaciation (Madeleine et al., 2009). The plateau is Early to Middle Noachian

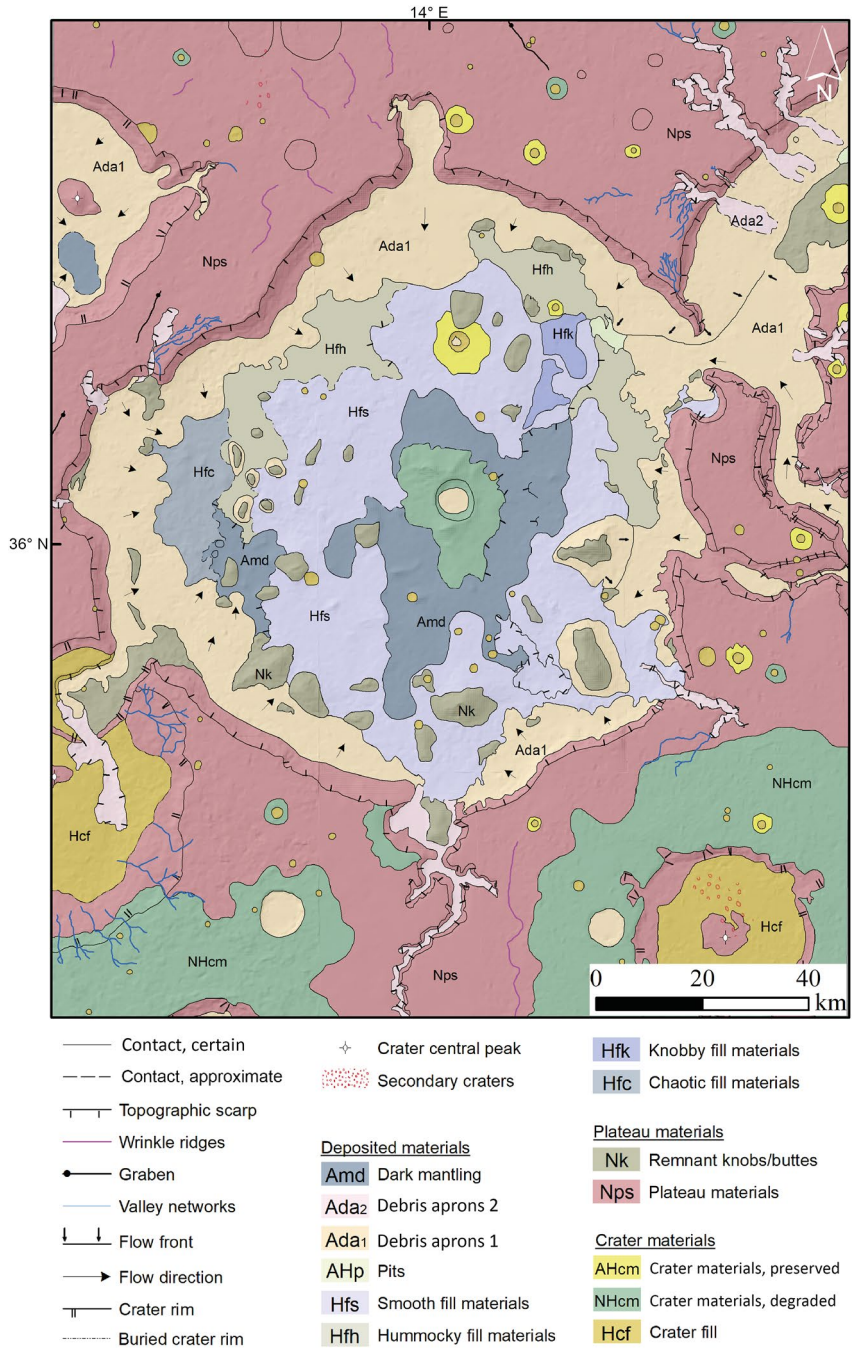

Figure 4. Geologic map of the research area at 1:1M print scale superposed on a HRSC-MOLA hillshade basemap. The hillshade map without the unit colors is included in the Appendix A (Figure A2) to highlight the linear features, their distribution, and their relationships.

in age and was formed in a period of high impact rates (Chuang & Crown, 2009; Tanaka et al., 2005). Thus, the unit has been modified by numerous impacts, forming a regolith layer that has covered secondary erosional/depositional and tectonic features. Effusive lava flows from unknown sources of Late Noachian to Early Hesperian age were superposed by aeolian sediments and/or impact breccia. Where the highlands are intersected by craters, depressions, or Mamers Valles, a potentially volcanic layer is exposed on the slopes (Figure 6). Since the layer protrudes from the slopes, the dark layer has to be more resistant than the overlying friable materials and could be part of the Martian volcanic plains (e.g., the regional basalt deposit, McGill, 2000). This provides strong evidence that the plateau is composed of a sequence of coherent lava flows, and then mantled by the

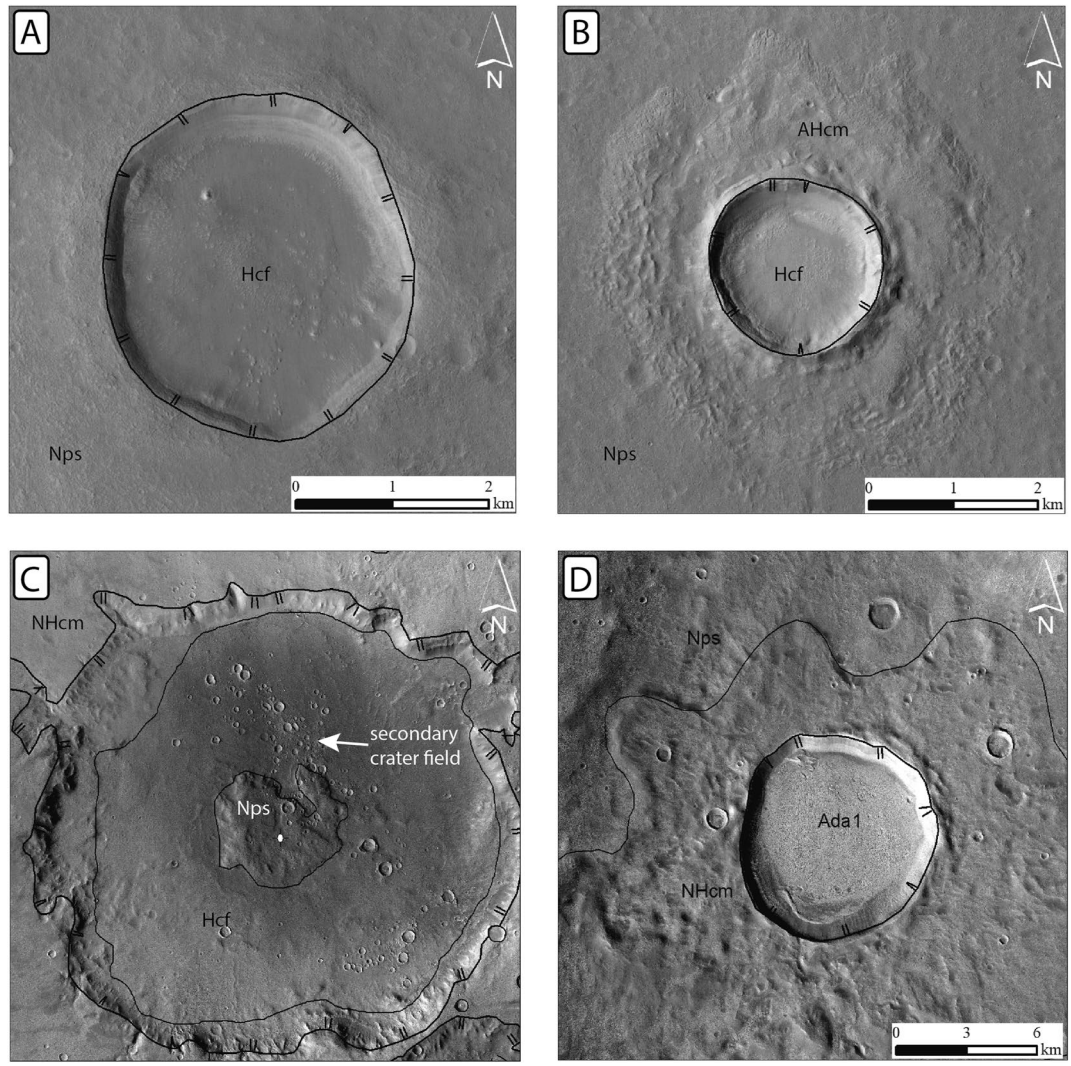

Figure 5. Comparison between (a) degraded/absent ejecta and (b) well-preserved pedestal ejecta blankets (AHcm) in CTX mosaics, (c) crater fill (Hcf) with smooth texture and secondary crater fields (indicated by the white arrow) within a degraded crater, and (d) debris aprons (Ada_1) covering the crater floor of a crater with lobate ejecta that has undergone deflation. Reference map Figure A1 in Appendix A.

180–300 m thick regional plains light surface layer (Figure 6). The ~50 m thick dark layer, serves as an important marker bed within our plateau unit (Nps), is covered by impact breccia, erosional products of the volcanic plains, and most importantly, sublimation residue from dust associated with the Amazonian plateau glaciation snowfall (Madeleine et al., 2009). Wrinkle ridges formed due to lava flow loading and regional tectonism support the presence of past volcanic processes and emplacement of regional volcanic plains. Graben in the region are oriented perpendicular to the wrinkle ridges and were formed by tectonic stresses (mostly straight graben), while sinuous rilles may have formed by thermal erosion or collapsing lava tubes. As a result of the burial of the volcanic plain by several hundred meters of light surface plain materials, possibly derived from the lag deposits of the Amazonian Plateau glaciation, ridges and graben both show an enhanced degradation state and a mantled morphology, similar to those seen in the mantled Hesperian ridged plains in the northern lowlands (e.g., Head et al., 2002). The underlying outcropping dark layers of possible ancient lava flows are recognizable where aeolian and fluvial processes eroded the fine light surface plains. Old craters were filled by lava flooding and fine aeolian transported materials, as can be seen in THEMIS-IR nighttime data. (Peri-)glacial processes within the valleys and/or melting of plateau-covering ice sheets led to parts of the plateau unit becoming unstable, dissect, forming floes, and

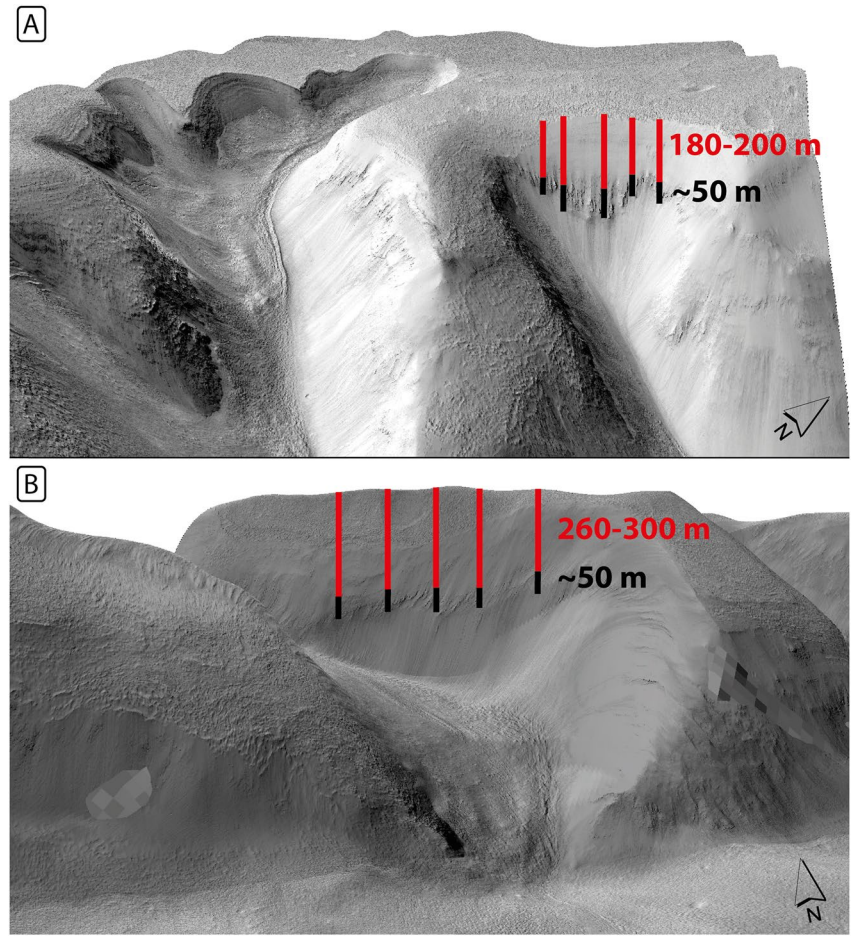

Figure 6. Oblique 3D view and thickness measurements of two outcrops of the dark volcanic marker bed (black column) and the overlying light surface layer (red column) located in panel (a) an alcove wall in the western part of the cavi (sun is coming from the south) and (b) in the northern wall of Mamers Valles (sun is coming from the west). The measurements were performed on HiRISE images ESP_036106_2170 and ESP_036884_2175 ((a, b), respectively) draped over the HRSC-MOLA Blended DEM. Reference map Figure A1 in Appendix A.

tipping into the valley. This process could be part of the evidence to better understand the nature and origin of the fretted terrain along the Mamers Valles.

Observed morphologies of branching channels associated with the alcoves indicate no relation to the Late Noachian—Early Hesperian valley network systems mapped globally by Hynek et al. (2010) and dated by Fassett and Head (2011). Instead, based on their sharp rims, they appear to be more recent and may be related to glaciation and changing climatic conditions, either through subglacial melt water runoff (Grau Galofre et al., 2020) under an ice sheet that covered much of the highlands (Fastook & Head, 2015; Fastook et al., 2014; Head et al., 2003, 2005), or by surface water runoff. Possible mechanisms for generating surface water runoff include either a warmer climate (Craddock & Howard, 2002; Hynek et al., 2010; Lamb et al., 2006) or melting of snow in the Amazonian and runoff during the waning period of a high-obliquity glaciation phase in the mid-latitudes. However, the branching fluvial channels are clearly superposed on the volcanic plains and the upper mantle unit, and thus are of a different age and origin than the traditional valley networks; therefore, we suggest that melt water in the waning period of the plateau glaciation formed the branching fluvial channels.

Nk—Remnant knobs/buttes—Remnant mounds are located inside Deuteronilus Cavus and within Mamers Valles. They stand out from their surrounding areas due to their morphology and topographic elevation. In particular, the southern part of Deuteronilus Cavus contains remnants up to more than 10 km in length. In the western part, there is an accumulation of small remnants with a length of only a few kilometers. Their heights show distinct variations, varying from a few 100 m up to a few kilometers above the surrounding terrain. The map shapes of the

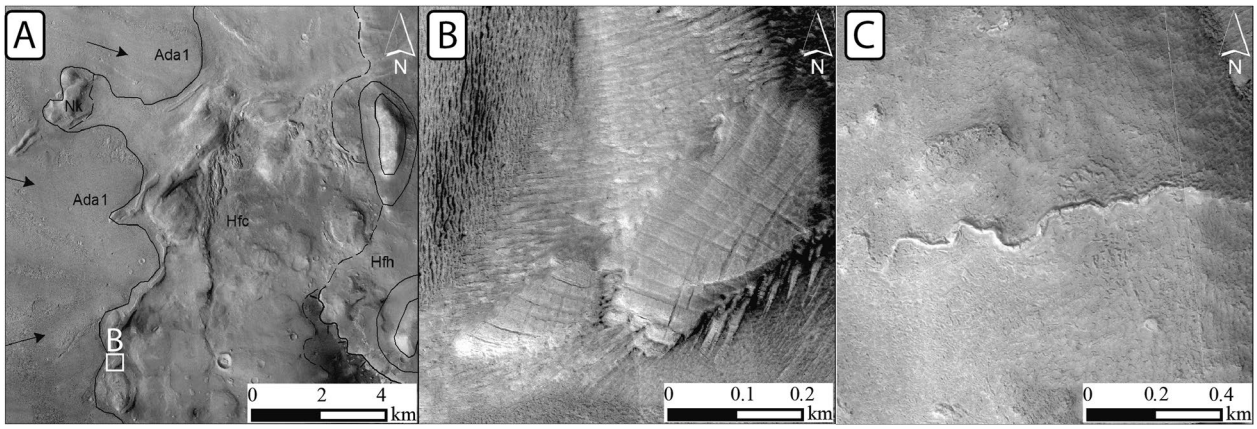

Figure 7. (a) Rough, ridged, and fractured morphology of the chaotic fill materials (Hfc) shown in the CTX mosaic and (b) surficial polygonal fractures observed on the finer grained materials on HiRISE image ESP_056664_2165. Inverted sinuous ridges of ∼1 km length (C, HiRISE image ESP_056664_2165) in the hummocky materials on the cavi floor (Hfh). Reference map Figure A1 in Appendix A.

remnants vary from roundish to angular and often appear to have irregular outlines. In cross-section the summits are rounded and the slope angles of the sides are steep. A large number of remnant knobs are surrounded by circumferential deposits. Stratigraphically, they occur in the Mamers Valles or in the smooth materials (Hfs) that fill the cavi floor, but it is unclear if the remnant knobs (Nk) overlie the fill materials or if they were embedded in the fill materials.

Interpretation: We interpret the remnant knobs as previous components of the Noachian plateau material. Their dissection from the plateau unit is either directly linked to the formation process of Deuteronilus Cavus or was initiated by volatiles in the plateau unit leading to destabilization and dissection along the edges. Since the distribution of remnant knobs is irregular and not only linked to Deuteronilus Cavus, it is more likely that parts of the Noachian plateau were dissected alongside structural weakness. They formed in the Late Noachian or in the Early Hesperian as they show advanced stages of degradation and are embedded in Hesperian fill materials. Furthermore, remnant knobs are often surrounded or enclosed by LDA, implying that they were once covered by icy materials and that ice played an essential role in their modification. Accordingly, the debris included in the LDAs is interpreted to consist of eroded material from the plateau and from the knobs. In general, Nk inside the cavi are most likely degraded wall slumps related to the original depression, while Nk outside the cavi are most likely linked to either the widening of the fretted channels in the Late Noachian-Early Hesperian (McGill, 2000) or to the Amazonian-aged lobate and lineated material that currently fills many of the fretted channels (McGill, 2000).

4.1.2. Fill Materials

Hfc—Chaotic fill materials—The chaotic terrain is located exclusively in the western part of Deuteronilus Cavus between Ada_1 and other fill units in topographical lows (Figure 7a). Within the unit, different morphologies and surface structures are exposed. Smoother materials are located in topographic lows in the center of the unit and are surrounded by a rougher, ridged and fractured material, which partly shows nearly rectangular polygonal fractures (Figure 7b). THEMIS IR-nighttime data reveal a lower thermal emissivity of the smoother materials as compared to the surrounding materials.

Interpretation: On the basis of its stratigraphic relationship to Ada_1 and its lobate morphology, we interpret the chaotic material as a strongly degraded, more extensive apron underlying the younger, well-preserved LDA. This scenario would imply different stages of glaciation in Martian history. Polygonal fractures are caused by thermal contraction of ice-rich apron materials (Mangold, 2011), but in this case are much more rectangular than other Martian polygons (Figure 7b). As the thermal emission is relatively low, it is likely that the lobate and degraded apron materials still contain some amount of ice, while the smoother materials are nearly ice-free dusty materials. However, the relationship to the Hfh unit remains unclear, but there is some evidence for a close temporal correlation between these two units based on their similar stratigraphic position (Figure 9).

Hfh—Hummocky fill materials—The hummocky surface is stratigraphically located between viscous flow materials (Ada_1, Ada_2) and smooth fill materials (Hfs), where the contact is characterized by a topographic

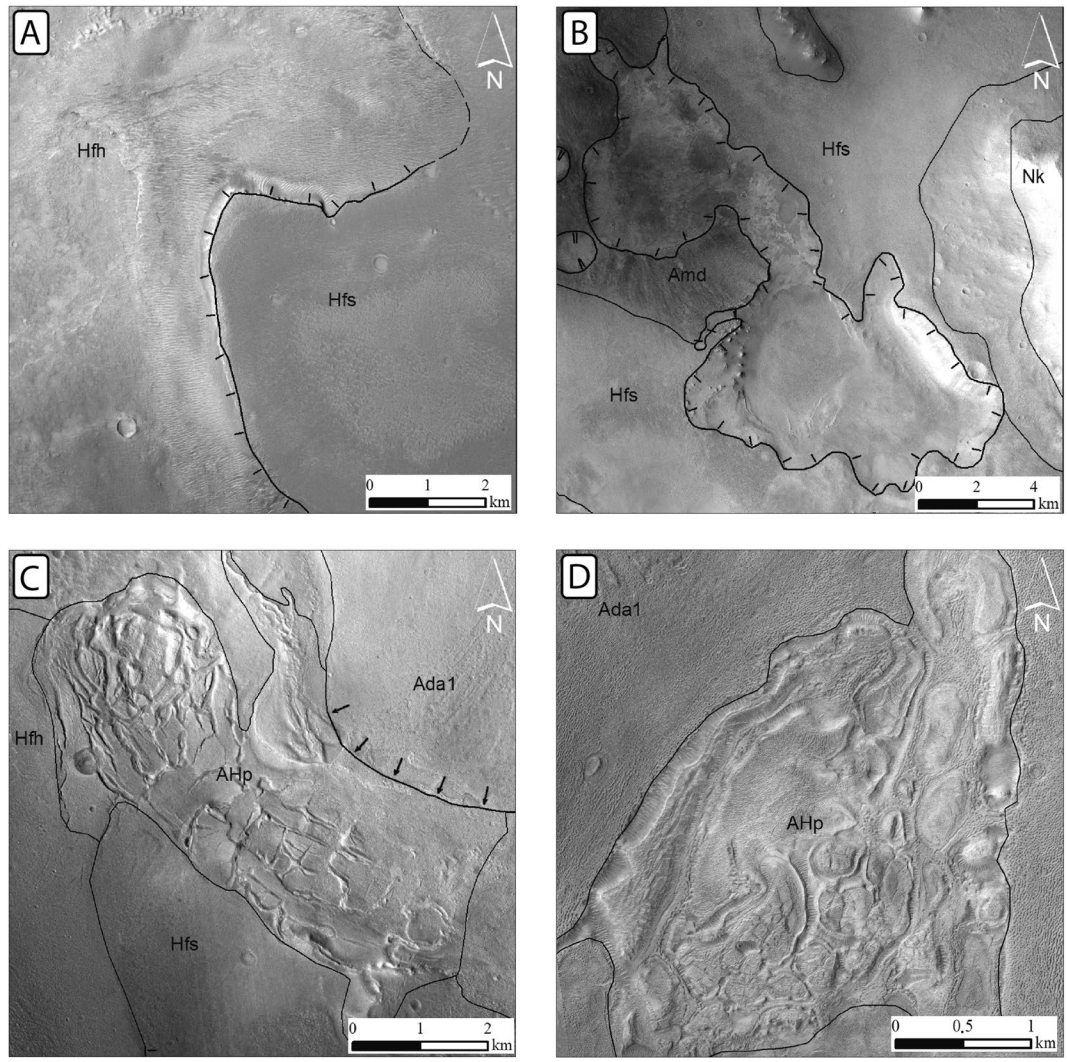

Figure 8. (a) Smooth fill materials (Hfs) affected by erosion and superimposed on hummocky fill materials (Hfh). (b) Subcircular depressions within Hfs show variable brightness of deposits in the CTX mosaic, and two types of pits (AHp): a polygonal fractured pit within Deuteronilus Cavus is shown in the CTX mosaic (c). And (d) between two merging lobate debris aprons in Mamers Valles with anisometric fracture pattern (HiRISE image ESP_043306_2175). Reference map Figure A1 in Appendix A.

scarp (Figure 8a). Fine-grained materials cover the unit's surface and form dunes along the scarp. Crater densities appear to be higher compared to Hfs, and smaller craters with raised rims are more common. The relative brightness varies from dark, smoother areas to bright, patchy and undulating areas. Surficial modification is partially observed but less distinctive compared to smooth fill materials (Hfs). Less than 100 m wide inverted sinuous ridges ranging in length from ~5 km (36.460°N, 13.250°E) to ~1 km (36.055°N, 12.945°E) with distinct morphology can be found within the hummock fill materials (Hfh).

Interpretation: Hummocky fill is an older deposit covered by younger smooth fill materials (Hfs). The stratigraphy is inferred by the higher crater density of Hfh compared to Hfs, the erosion of Hfs to create the scarp, and the presence of inverted sinuous ridges in the Hfh unit (Figure 7c). Erosion by aeolian or fluvial/periglacial processes exposed the older, hummocky materials of unit Hfh beneath (Figures 3b and 9). The erosional contact between Hfh and Hfs is defined by a topographic scarp (Figure 8a). The deposition of the hummocky, mass-wasted detritus occurred during the degradation of the plateau materials (Nps) in the Hesperian period and was subsequently covered by younger, smoother deposits of unit Hfs. The inverted sinuous ridges are interpreted as inverted

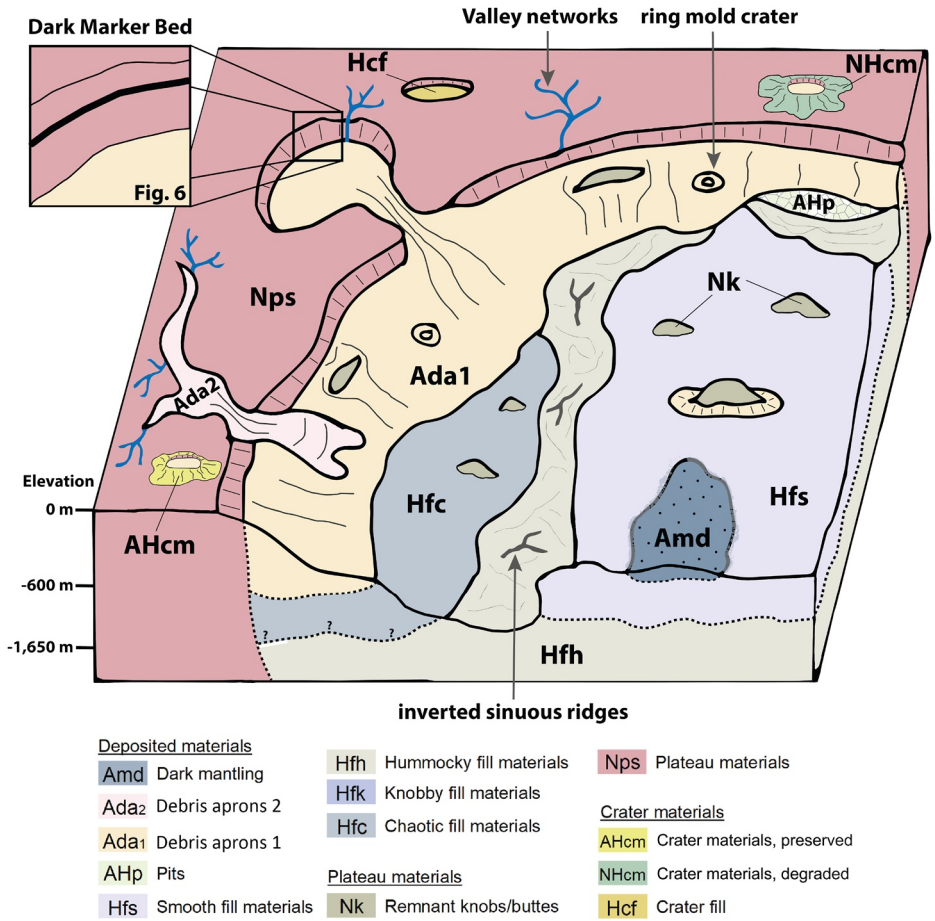

Figure 9. Interpretative block diagram to illustrate the geological relationships of selected map units (schematically).

sinuous channels associated with meltwater ponding on the surface of the cavus during the waning period of a high-glacial phase or as eskers of subglacial channels.

Hfk—Knobby fill materials—The spatial distribution of knobby materials is restricted to the northeastern part of Deuteronilus Cavus. The unit forms an elevated surface with scarps defining its south and west margins. Along the scarps, parts of the plateau are dissected and several parallel fractures are visible in plain view. The unit is characterized by clusters of knobs covered by sharp-edged boulders (~3–6 m in diameter) and surrounded by dunes (Figure 10c).

Interpretation: There are two possible processes that are candidates to explain the formation of the knobby materials (Hfk). Erosion of an upper layer can leave circular knobs and boulders behind as deflation removes finer materials in between. Alternatively, the unit was once formed by or covered by an ice sheet that incorporated rocky fragments. During the sublimation and retreat of the ice the rock fragments were deposited as boulders on the current surface. In addition, the observed boulders appear to have undergone minimal transport, as they are not rounded. Thus, the materials might be the sublimation remnant of a former debris-covered ice sheet surface or the remnant part of the terrain at the base of the crater wall. The numerous parallel fractures along the scarp formed as a consequence of the accumulated tension due to the relief.

Hfs—Smooth fill materials—Flat-lying smooth textured materials with variable relative brightness mantle large parts of Deuteronilus Cavus. The relatively featureless materials are located next to hummocky/knobby (Hfh/Hfk) and low relative brightness materials (Amd) in topographic lows. The smooth fill materials (Hfs) surround remnants, located within the unit, and are in some places covered by viscous flow materials. The unit exhibits sub-circular depressions (Figure 8b, e.g., 35.7°N, 14.3°E) with layered floors, variable brightness, and evidence for phyllosilicates (Morgan et al., 2021). Crater densities are lower than on the highland materials and craters

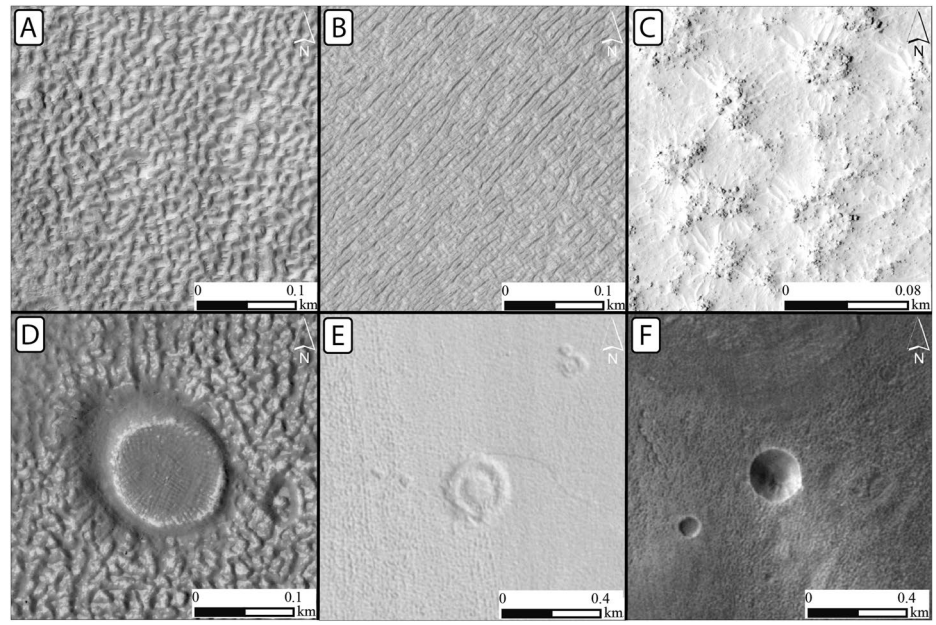

Figure 10. (a) Brain-terrain texture (HiRISE image ESP_043306_2175), (b) lineated texture (aligned mounds and pits, HiRISE image ESP_036106_2170) in Ada_1 unit, (c) clusters of boulders covering the knobby fill materials (Hfk) surrounded by dunes (HiRISE image ESP_026625_2165), (d) ring mold crater with central plateau (HiRISE image ESP_033785_2175), (e) multi-ring crater (CTX mosaic) on the Ada_1 unit are indicative for the presence of ice in the lobate debris aprons (LDA)/ lineated valley fill (LVF), and (f) a bowl-shaped crater (CTX mosaic) superposing the LDA/LVF can be used to estimate the minimum till thickness (Kress & Head, 2008).

typically lack ejecta blankets and pronounced rims. Dunes are visible and sometimes accompanied by dark streaks that extend beyond the contact and into the unit Amd.

Interpretation: The origin of this material is related to the erosion of highland material (Nps) and deposition in low-lying parts of Deuteronilus Cavus (Figure 8b). Tanaka et al. (2005) proposed a Hesperian age for the smooth fill materials (Hfs). Aeolian activity results in the filling of craters, formation of dunes, and wind streaks. The smooth fill materials are affected by erosion as a topographic scarp defines the contact between Hfh and Hfs (Figure 8a), and erosional material is deposited on the lower side (Hfh) of the scarp (Figure 9). Sub-circular, layered depressions bearing Fe-Mg-phyllosilicates (Morgan et al., 2021), imply the presence of surface/groundwater in the past, or may possibly be related to excavation during the Cavi-forming impact (e.g., Sun & Milliken, 2015) and later redistribution. Phyllosilicate-bearing units are also present in the Ismenius Cavus depression that is connected to Mamers Valles as well (Dehouck et al., 2010) and are discussed in Section 5.3.

AHp—Pits—The unit exhibits unique surface textures and morphologies spatially associated with the distribution of glacial and periglacial landforms and is limited to two small areas, one within Deuteronilus Cavus and one in Mamers Valles (Figures 8c and 8d). In both cases, the pits (AHp) are located at the flow fronts of the LDAs. In the cavus, polygonal and circular fractures have formed separating plateaus, resulting in a high-relief pit floor. The fractures in the Mamers Valles pit show an anisometric pattern with curvilinear ridge and trough textures (Figure 8d).

Interpretation: This unit was possibly formed by the sublimation of sub-surface ice, forming surficial fractures (Mc Keown et al., 2017). The absence of an angular fracture pattern in Mamers Valles (Figure 8d) might be the result of subsequent material movement after sublimation took place or ice sublimation over pre-existing landforms (Mangold, 2011). Since the occurrence of this unit is spatially associated with viscous flow fronts of unit Ada_1 (Figures 8c and 8d), the flow front of the uppermost apron may be less covered with debris and therefore affected by active sublimation. Another possibility is that the pits were formed by the sublimation of ice incorporated into an older, underlying apron (similar to Hfc).

Ada_1—Debris aprons 1—LDAs, extending ~5–30 km from the base of steep slopes into lowlands, and LVF were mapped as the same unit (Ada_1) as both show similar behavior and texture and do not allow a conclusive

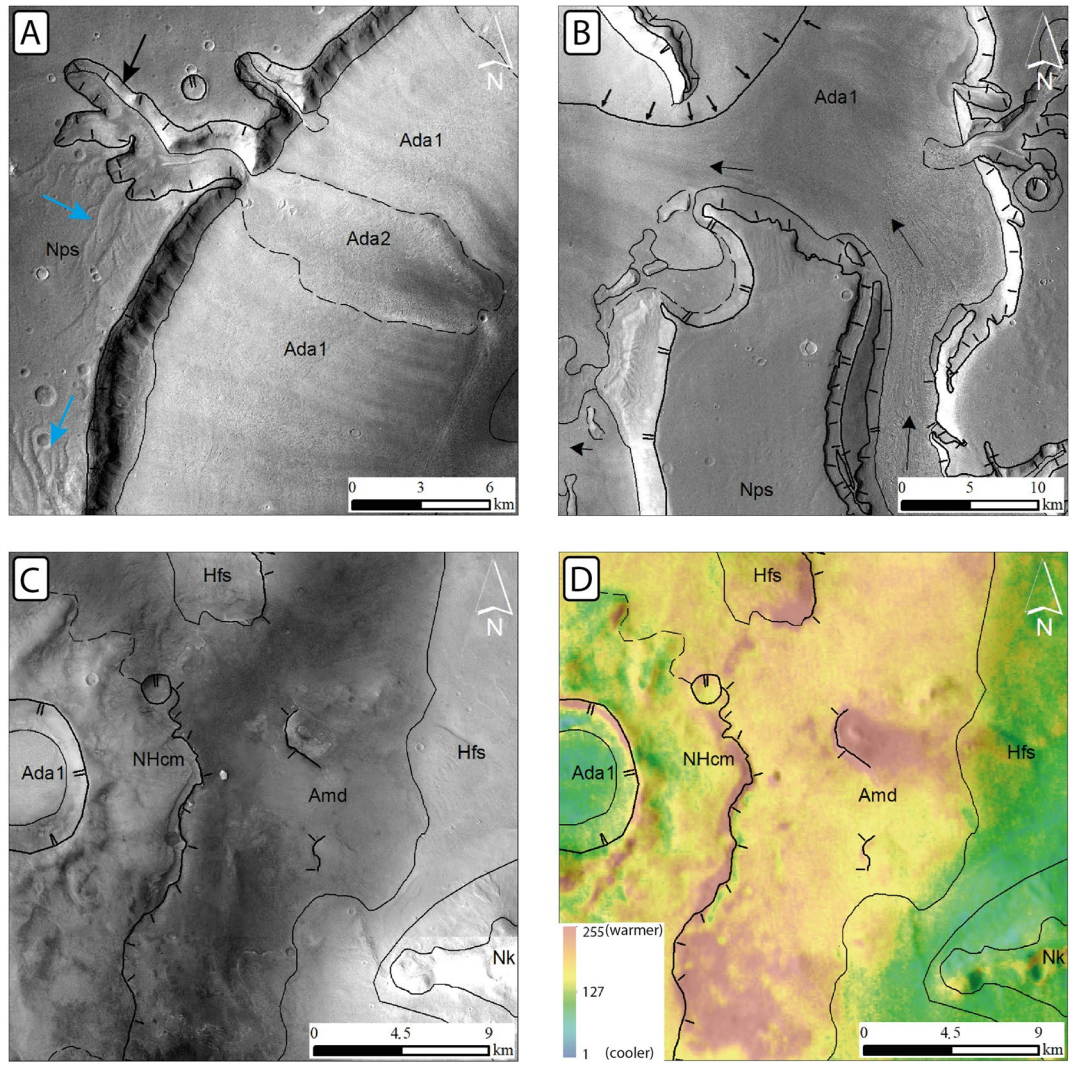

Figure 11. (a) Branching fluvial channels on the plateau (blue arrow) and a sharply defined alcove (black arrow) with extending lobate debris aprons (LDA) (Ada_2) superposing older Ada_1 (CTX mosaic), (b) surficial striations with indicated flow directions (arrows) and flow fronts (small arrows pointing toward the line) of Ada_1 show that Mamers Valles LDA/lineated valley fill (right) is flowing into Deuteronilus Cavus (left, CTX mosaic); dark mantling materials (Amd) appear dark in the CTX mosaic (c) and have high thermal emission compared to adjacent units revealed by THEMIS-IR nighttime data (d). Reference map Figure A1 in Appendix A.

differentiation. In addition, most of the isolated remnant knobs (Nk) within Deuteronilus Cavus are surrounded by circumferential LDAs. In order to show coalesced valley wall LDAs turning downslope to form LVF, flow direction and flow fronts were incorporated into our geologic map when visible (Figure 4). Surficial striations perpendicular to the scarp or parallel to it diverge around obstacles located in the path of flow (Figure 11b). In valleys, striations are preferentially oriented parallel to the valley walls. By visual observation, crater density and morphology are similar to Ada_2, exhibiting ring mold craters with a central plateau (Figure 10d) or multiple rings (Figure 10e), and bowl-shaped craters (Figure 10f) 50–200 m in diameter. Surface textures of the flows vary from lineated alternating ridges and pits, called "sandpaper-like" by Carr (2006), toward interconnected and alternating sinuous troughs and ridges, called "brain-terrain texture" (Levy et al., 2009; Figures 10a and 10b). The parallel lineated sharp ridges are less than 10 m in thickness and vary in length. In contrast, the sinuous ridges are up to 20 m thick, more rounded, and show cellular texture.

Interpretation: Plaut et al. (2009), using SHARAD radar data, showed that LDA in the Martian mid-latitudes were debris-covered glaciers consisting of >80% ice, which is covered by a layer of protective sublimation lag

deposits less than about 20 m thick. In addition, the crater morphology can be used to further estimate the thickness of the overlying lag deposits, since ring mold craters (Kress & Head, 2008), such as those with a central plateau or multiple rings, are characteristic of impacts that penetrated through the regolith till into the glacial ice, whereas bowl-shaped craters did not reach the underlying ice. Therefore, by calculating the excavation depth from the bowl-shaped crater diameters according to Croft (1981) and Kato et al. (1995), we can estimate the minimum thickness of the regolith till. Kress and Head (2008) derived an average regolith layer thickness of ∼15 m for a mean bowl-shaped crater diameter of ∼77 m in Mamers Valles. In our study area, the mean bowl-shaped crater diameter is ∼86 m, yielding an average regolith layer thickness of ∼17 m. However, we suggest that the regolith layer is heterogeneous in thickness. Thus, it may be thinner in some places and thicker in others, as indicated by the largest bowl-shaped crater (Figure 10f), which has a diameter of ∼318 m, suggesting a local ∼64 m thick protective regolith layer above the glacial ice. Since this crater is located in the center of Mamers Valles, where LDAs from opposite valley walls coalesced, it is most likely that till covering the glacial ice accumulated in these zones. Surficial striations and divergence around obstacles indicate viscous flow of materials and can be used to establish flow directions (Head et al., 2005, 2006). In addition, the irregular shape of pits is indicative of sublimation of incorporated ice (Baker & Head, 2015). To establish viscous flow of the glacial landforms, at least 28 wt.% of ice is needed (Mangold et al., 2002).

There are, however, different hypothesis for the source of incorporated ice: (a) Lucchitta (1984) suggested pervasive ground ice in these latitudes that becomes incorporated in talus resulting in mobilization to form ice-cemented debris flows, (b) Hamlin et al. (2000) proposed water discharging from a regional aquifer as a source of ice, and (c) Head et al. (2005) proposed that LDA are glaciers emerging from snow and ice accumulation in alcoves. In periods of higher obliquity, enhanced precipitation of snow and accumulation of ice on plateaus and in alcoves (Madeleine et al., 2009) leads to the formation of glaciers (Head et al., 2005). The surface textures of these glaciers change due to variable ratios of ice and debris, differences in the thickness of superposed lag deposits, and different illumination geometry of the surficial materials. In our research area, two LDAs extending from opposite valley walls merge in the valley center, as indicated by the flow front signature in our map (Figure 11b). In the center of the valley or similarly confined spaces, the surface lineations are generally parallel to the valley walls and to the flow direction, which are the characteristics of LVF. Consequently, we favor the formation mechanism proposed by Head et al. (2005), in which the glaciers were formed by snow precipitation and ice accumulation and flow on plateaus and in alcoves. Furthermore, we propose that LDA and LVF are two morphological end members of features formed from the same material, and no conclusive distinction between these two end members is visible in our study area. Apron ages are difficult to determine due to ongoing modification processes and continuous destruction of smaller craters (Mangold, 2003). As a consequence, derived ages differ from several hundred million years to a few million years (Head et al., 2006; Mangold, 2003) but are all well within the Amazonian period (Figure 13).

Ada_2—Debris aprons 2—Alcoves are present at the margins of the plateaus and filled by LDAs extending downwards into Deuteronilus Cavus and Mamers Valles. The contact between the alcove and the plateau is sharply defined and branching channels drain toward the alcoves (Figure 11a, see also Figure 6a, left, for a perspective view). Ada_2 superposes Ada_1, shows surface striations with preferential orientation parallel to the curvature of valleys and rims, shows low thermal emissivity in THEMIS-IR nighttime data, and forms higher lobate flow fronts superposing and cross-cutting the Ada_1 features. Small craters (<0.5 km) with an elongated shape parallel to the slope are common, while larger craters are rare.

Interpretation: Debris aprons consisting of ice and mass-wasted detritus that flowed downwards and covered older units. Superposition of Ada_1 by Ada_2 highlights two periods of emplacement of viscous flow materials, with changing climatic conditions in between, also suggested by Morgan et al. (2009) for the nearby DM region. Since the crater densities are low in both units, they are assumed to have similar young ages. Ada_2 is Amazonian-aged, although age determinations are difficult due to the active obliteration of smaller craters (Carr, 2006). We interpret the first glacial stage in the area to be represented by an extensive plateau glaciation, of which the LDA and LVF (Ada_1), which cover most of the cavi and valley floor (Figure 4), are the remnants of the receding plateau ice sheet at the end of the glacial period. Their morphology and texture indicate viscous flow downslope from the cavi/valley walls and along the Mamers Valles toward the north (Figure 11b). The subsequent glacial stage was less extensive and is characterized by LDA (Ada_2) emerging from cavi/valleys and superimposed arcuate lobes on the remnants of the first glacial stage (Figure 11a). These features also contain a record of viscous flow, but are significantly smaller with extensions of less than

12 km from the walls into the valley or cavi. To accurately measure the stages of glaciation over time and space, in-depth analysis of the LDA and LVF in the cavi and Mamers Valles is necessary. This should include examination of variations in texture and morphology, superimposed craters, and the relationship between glacial features from different epochs. Such studies will provide valuable data to refine precise climate models for the glaciation phases.

Amd—Dark mantling—Materials with significantly lower brightness in the CTX mosaic compared to other units (Figure 11c) are distributed in the central part of Deuteronilus Cavus and in the south of the northwestern crater within the research area. The dark materials are partly associated with, but not limited to, topographic depressions (Figures 3a and 3b). THEMIS IR-nighttime data reveal relatively high thermal emission compared to other mapped units (Figure 11d). Furthermore, dark streaks without preferred orientation extend beyond unit boundaries. The dark mantling layers are partially thin enough to show the textures of the underlying units, whereas other parts of the mantling suggest the accumulation of more materials resulting in a thicker dark layer. The unit is deficient in young craters, whereas some old craters are partially covered by the dark material.

Interpretation: The dark mantling materials are interpreted as aeolian deposits accumulated in depressions (Figure 9) and reworked by aeolian activity. Since the occurrence is not restricted to a specific topographic level, dark materials cover small mounds, and the contact with adjacent units is gradual, it is unlikely that the dark materials originate from exhumed bedrock. Instead, the material could be either volcanic ash of unknown source, weathered rock debris mobilized from the debris cover deposits by aeolian activity, or a mixture of both (Noe Dobrea et al., 2010). Dust devil tracks causing the modification of the uppermost surface layer also indicate recent aeolian activity (Fergason & Christensen, 2008). The deposition of dark materials in the southeast of the northwestern crater may point to a preferred wind orientation from NW to SE. Since the dark materials mantle Amazonian LDAs (Ada_1), their depositional activity is very young. The relatively high signal in THEMIS IR-nighttime (Figure 11d) is attributable to the higher thermal inertia of mafic material weathered from the volcanic caprock. Furthermore, spectral evidence for Fe-Mg phyllosilicates and Al-rich phyllosilicates (Morgan et al., 2021) partially correlates with the distribution of the dark mantling but is not restricted to this unit as the CRISM data also show evidence for phyllosilicates on the smooth fill materials (Hfs; Figure 14b).

4.1.3. Crater Materials

Hcf—Crater fill—Most of the crater floors are covered by a deposit with a smooth texture. In some parts, patches of hummocky surface texture, secondary craters, low relative brightness mantling, and dunes are observable. The hummocky texture is prevalent in the western section of the crater floor and situated near the crater rims. The crater fill is moderately cratered and sometimes superposed by LDAs (Ada_1) extending downward from the crater walls (Figures 5c and 5d).

Interpretation: The craters were filled during the Hesperian period by aeolian materials and mass-wasted detritus. The hummocky texture is caused by remnants and debris of the plateau that collapsed from the crater wall. These materials were later covered by mantling materials, resulting in their blurred morphology. The crater fill materials were affected by the formation of secondary craters and modified by aeolian activity forming dunes.

NHcm—Crater materials, degraded—Crater rims are semi-continuous when compared to AHcm, ejecta blankets show less relief with respect to the surrounding units, and a pitted surface (Figure 5a). In addition, the larger craters are partly superposed by younger craters. Crater walls are partly cut by branching channels and are heavily eroded (southwestern part of our study area, Figures 4 and A2). Some crater floors exhibit a smooth crater fill (Hcf) and secondary craters, which are identified by their non-circular and overlapping shape, their clustered distribution, and their similar degree of degradation (Figure 5c).

Interpretation: Crater materials of Hesperian to Noachian age are moderately to highly degraded. Based on the presence of ejecta and branching fluvial channels cutting through the crater walls, these craters can be classified as Type II according to the crater degradation scheme (Mangold et al., 2012). Additionally, deflation has altered the ejecta, leading to its pitted appearance.

AHcm—Crater materials, preserved—Craters with continuous rims and significant relief with respect to surrounding units are common. The ejecta blankets of these craters show distinctive margins, and are not superposed by younger craters (Figure 5b). Several, but not the majority, of the craters in this category show lobate (Figure 5d) or pedestal ejecta (Figure 5b).

Interpretation: Well-preserved crater materials with little degradation form ejecta blankets and crater rims of the Amazonian to Late Hesperian Age. Based on well-defined ejecta blankets and the absence of fluvial landforms, these craters can be classified as Type III according to the crater degradation scheme (Mangold et al., 2012). The presence of lobate and pedestal ejecta blankets indicates the presence of (sub)surface ice during the crater formation (Weiss & Head, 2015) in the Early Hesperian/Amazonian. This suggests a glaciation phase covering the plateau unit in the Amazonian as the lobate and pedestal craters are well defined and fresh (Figures 5b and 5d).

4.2. Correlation of Mapped Units

Based on superposition relationships, relative crater densities derived ages from previous studies (Baker & Head, 2015; Carr, 2006; Chuang & Crown, 2009; Head et al., 2006; Mangold, 2003; Mangold et al., 2012; Tanaka et al., 2005, 2014), and the interpreted climate conditions throughout Martian history, we have constructed a correlation chart of our mapped units (Figure 12). Absolute period extents are based on Ivanov (2001), Hartmann (2005) and Hiesinger and Tanaka (2020). Note that exhumed units are arranged and labeled according to their interpreted deposition/formation age rather than their exhumation age.

The Noachian plateau materials (Nps) are a mixture of volcanic deposits and their erosional products, indicated by internal layering and wrinkle ridges, which were reworked by impacts. The Hesperian-aged deposits within Deuteronilus Cavus indicate that the formation of the cavus and the emplacement of remnant knobs/buttes (Nk) occurred in the Noachian period (Figures 13a and 13b). Stratigraphic relationships between Noachian plateaus (Nps) and branching fluvial channels spatially associated with alcoves suggest that the channels are more recent and are probably not related to the Late Noachian—Early Hesperian valley network systems mapped by Hynek et al. (2010) and dated by Fassett and Head (2011). In the Early Hesperian period, hummocky (Hfh) and chaotic (Hfc) fill materials were emplaced by mass-wasting processes. Later, in the Late Hesperian period, these deposits were covered by knobby fill materials, which include sharp-edged boulders (Hfk), and smooth fill materials (Hfs) that cover parts of the cavi's floor (Figure 13b). Erosion of the smooth deposit (Hfs) possibly in the Early Amazonian exhumed the underlying hummocky materials (Hfh), and the chaotic materials (Hfc) in the floor of Deuteronilus Cavus (Figure 9). The formation of sublimation-related landforms, for example, pits with polygonal fractures (AHp), indicates the presence of subsurface ice (Figure 14a). Crater materials formed from the

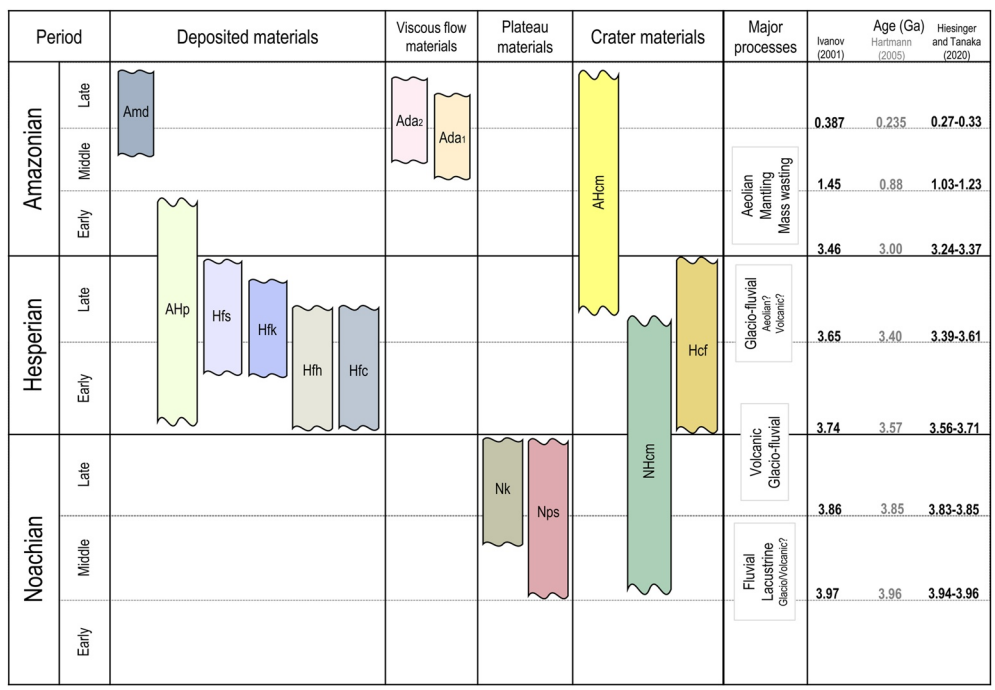

Figure 12. Correlation chart of map units defined in Figure 4. The cavi-forming impact occurred in the Noachian period, but the exact timing is challenging to reconstruct due to severe subsequent modification of the crater. The initial impact also sets the lower limit for the age of the Nk unit.

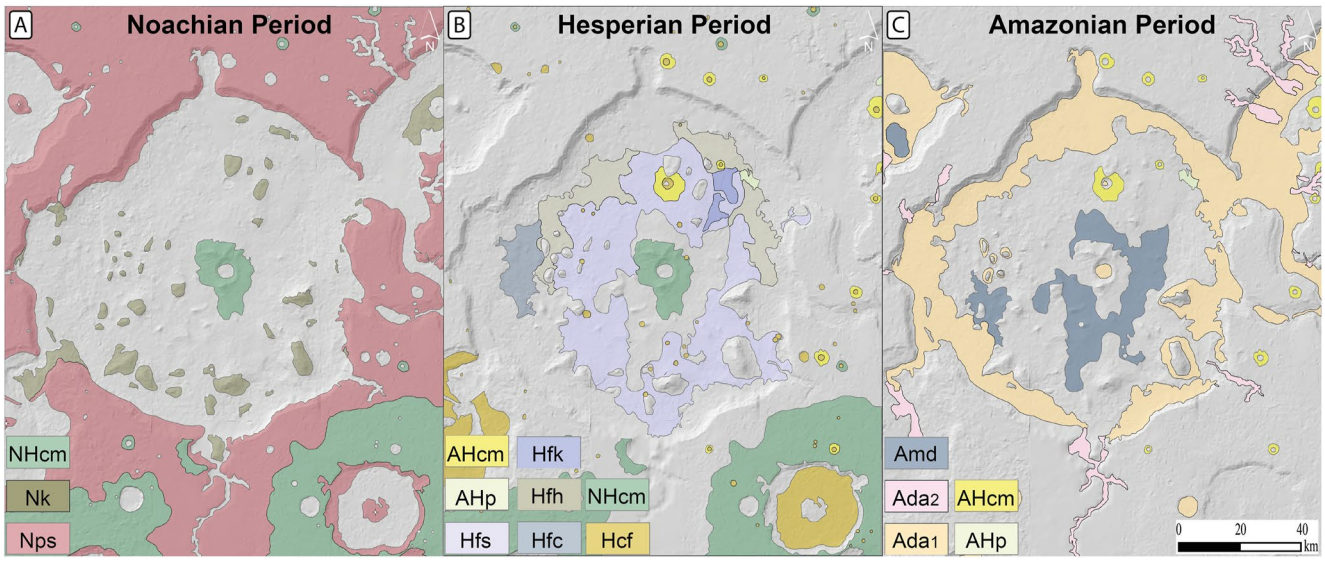

Figure 13. Spatial distribution of distinct stratigraphic units. (a) Noachian period units, (b) Hesperian period units, and (c) Amazonian period units with a HRSC-DEM hillshade basemap.

Noachian to the Early Hesperian (NHcm) are highly degraded and intersected by branching channels. Craters that are not filled by glacial landforms contain aeolian and mass-wasted Hesperian-aged deposits (Hcf) superposed by secondary craters. Glacial activity in the Middle and Late Amazonian led to the accumulation of LDAs and LVFs (Ada_1, Ada_2) at the base of steep slopes associated with craters, Deuteronilus Cavus, and Mamers Valles (Figure 13c). Glacial landforms are a result of global climatic processes, such as orbitally forced precipitation enhancement (Head et al., 2003). In a few places, younger glacial landforms (Ada_2) extend from alcoves and superpose older glacial landforms (Ada_1), suggesting two periods of glacial activity with changing climatic conditions in between. However, because crater densities are low on both units, they are probably similarly young. Craters formed since the Late Hesperian show less degradation than older crater materials (NHcm). They

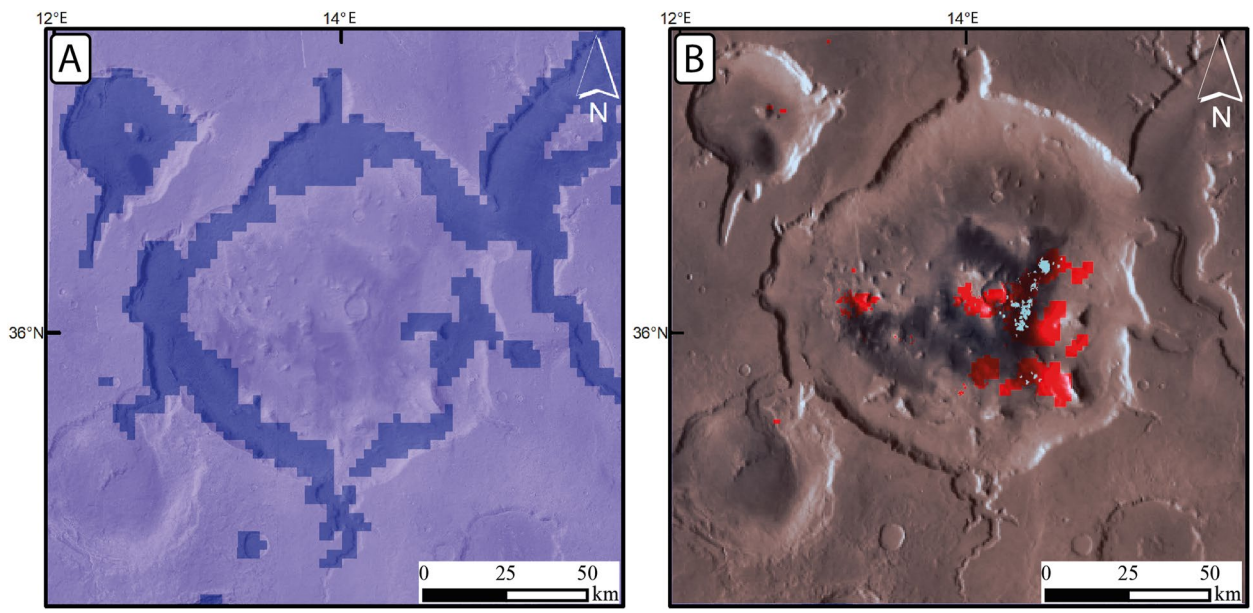

Figure 14. (a) Ice consistency (presence of shallow ice [<5 m] with high confidence (Morgan et al., 2021), dark blue) correlates with the distribution of glacial features in our map (Figure 4) and (b) evidence for Fe-Mg phyllosilicates (red) and Al-rich phyllosilicates or hydrated minerals (e.g., clay minerals) (blue) in CRISM data within our research area. Ice consistency and spectral data were obtained from the Subsurface Water Ice Mapping project's website (Morgan et al., 2021).

impacted into an ice-rich (sub)surface, as evidenced by lobate and pedestal ejecta blankets (Weiss & Head, 2015). While there is no genetic link between fluvial activity (Hesperian period) and glacial (Middle to Late Amazonian period) activity observed in Ismenius Cavus (Dehouck et al., 2010), the close correlation between fluvial channels, alcoves, and $Ada_{1,2}$ in our study area may suggest a causal relationship. Recent geologic activity is indicated by dunes and aeolian modification of dark, presumably volcanic, mantling materials (Amd), which accumulated in topographic lows in the Late Amazonian.

5. Discussion

5.1. Comparison to Previous Maps

Lucchitta (1978) produced a geological map of the Ismenius Lacus quadrangle (MC-5) based on Mariner 9 television experiment imagery at a scale of 1:5,000,000, as part of a map series covering the entire Martian surface. The lack of high-resolution topography and high-resolution imagery data, and the data defining the physical properties of the surface materials at that time limited the identification and interpretation of units, contacts, and stratigraphic relationships. With higher resolution data, we were able to improve the geologic mapping and interpretation of the geologic history. Lucchitta (1978) interpreted the floor materials in Mamers Valles as aeolian sand deposits covering alluvial materials, and the materials covering the cavis floor as volcanic flows. Dehouck et al. (2010), Greeley and Guest (1987), Tanaka et al. (2005), and this work interpret these deposits as volatile-rich mass-wasted detritus (Hfs, Hfh, Hfk, Hfc) containing significant amounts of ice enabling viscous flow (Ada_1, Ada_2).

In an analysis of the northern plains of Mars, Tanaka et al. (2005) produced a geologic map at 1:15,000,000 scale using MOLA, THEMIS, MOC, and Viking data sets. Tanaka et al. (2005) identified three individual units within our mapping area: the DM 2 unit (ABd_2) and the DM 1 unit (HBd_1), both interpreted to be ice-rich, and the Noachis Terra unit (Nn). These units represent the surrounding plateau materials, the Hesperian-aged deposits within Deuteronilus Cavus, and the Amazonian-aged glacial landforms (e.g., Ada_1 and Ada_2) in our geologic map. However, our comprehensive map further differentiates the deposits and glacial landforms. We were able to distinguish between a smooth (Hfs), a hummocky (Hfh), a knobby (Hfk), and a chaotic (Hfc) endmember of the Hesperian deposits, which fill Deuteronilus Cavus. Furthermore, we identified the exhumation of hummocky deposits (Hfh) through erosion of the flat-lying deposit (Hfs). In addition, we identified at least two periods of glacial activity (Ada_1 and Ada_2), highlighting changes in climate conditions in between.

5.2. Origin of Deuteronilus Cavus

The origin of the nearly circular Deuteronilus Cavus (~105 × ~120 km) within our research area is uncertain as the depression is connected to the Mamers Valles in the northeast, and to a ~50 km crater in the southwest (Figure 2). The formation is either induced by an ancient impact crater, which was modified by volatile-rich erosional processes, using supervolcanoes (Michalski & Bleacher, 2013), or is a product of erosional processes, such as thermokarst degradation and mass-wasting. The latter points to large-scale degradation of subsurface permafrost, possibly related to the formation of Mamers Valles, and to atmospheric deposition of ice-rich material in the Amazonian, which is recently subject to thermokarst degradation (van Gasselt et al., 2010). Michalski and Bleacher (2013) proposed that several irregularly shaped craters in Arabia Terra may have been formed by supervolcanoes. However, Deuteronilus Cavus lacks key morphological features of a volcanic caldera (e.g., low topographic relief, stratified deposits, lava lakes, or arcuate scarps and ridges surrounding the cavus; Michalski & Bleacher, 2013). In contrast, an impact origin could be responsible for the nearly circular shape of Deuteronilus Cavus, and subsequent erosion and mass-wasting processes driven by fluvial and glacial activity led to pervasive modification of the ancient crater. Additionally, Deuteronilus Cavus exhibits a peak that is superposed by an impact crater (Figure 4), and that is located approximately in the center of the cavi (Figures 3a and 3b). This peak feature is not well defined as it is heavily degraded, but could be considered an ancient central crater peak. However, the central peak is superposed by ejecta material, which is why it was mapped as crater materials (NHcm, Figure 4). Moreover, the nearly concentric distribution of remnant knobs/buttes (Nk) may indicate that this unit is an erosional residue of the ancient crater rim. Alternatively, rather than modification of one ancient crater, modification of two superposed impact craters could explain the different radius of curvature of the southern and northern rims. However, both processes (impact crater modification or thermokarst degradation)

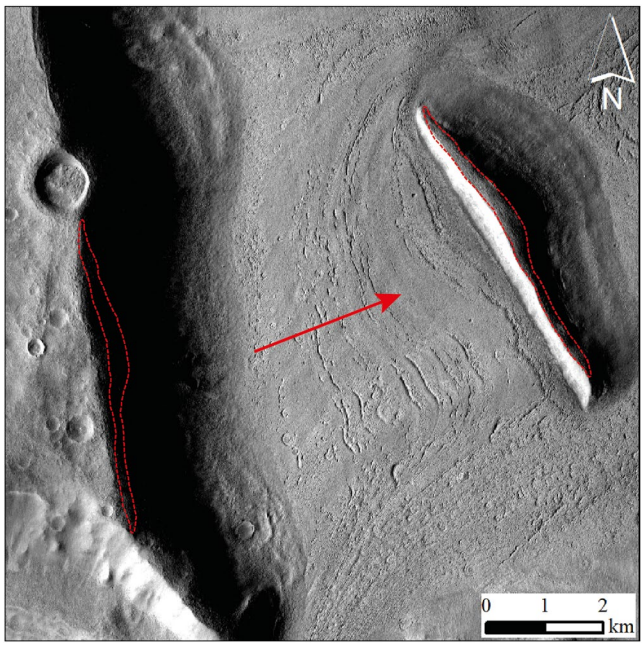

Figure 15. Example of a transported plateau block (right red dashed line, ~6 km long) that was transported ~7.5 km from the cavi wall. The shape of the dissected plateau block (Nk) matches the shape of the cavi rim (left red dashed line, CTX mosaic). The movement and rotation of the dissected plateau block (Nk) can be followed by the orientations of fissures in the glacial unit Ada_l. Reference map Figure A1 in Appendix A.

would form a complex depositional and erosional system, which is sensitive to cyclic climate variations.

Considering all scenarios, based on its generally circular shape, evidence of crater wall and rim erosion and retreat (Figure 15), and the presence of a prominent mound in the center of the cavi interpreted as a remnant central peak, we propose that pervasive erosional modification and enlargement of a pre-existing crater resulted in the present shape. The cavi-forming impact occurred in the Noachian period, but the exact timing is challenging to reconstruct due to severe subsequent modification of the initial crater. Erosional processes modifying craters that impact surface snow and ice deposits would include backwasting of material from the crater rim crest (Fastook & Head, 2014). Additionally, top-down-melting due to hot ejecta deposits (Kite et al., 2011) could generate melt water runoff and thereby erosion of the rim and fluvial channels intersecting the crater walls (Weiss & Head, 2015). In this scenario, the spatial connections of Deuteronilus Cavus to nearby valleys and craters are presumably a product of backwasting, top-down-melting of snow/ice, and widening of tributary valleys. The modification of an impact crater driven by glacial activity and backwasting can be observed at the ~50 km crater in the northwest of our mapping area (Figure 2), possibly representing the process of alteration and enlargement of a crater leading to its asymmetry and lack of characteristic features such as its circular shape or any discernible rim topography. Similar assumptions are made for Ismenius Cavus in the southeast of our mapping area (Dehouck et al., 2010).

To quantify the potential enlargement of the original crater, we calculated the original crater diameter using the alleged central peak diameter of ~18 km, retaining an original crater diameter of ~60 km (Garvin et al., 2003), implying an enlargement of 175%–200%. It should be noted that the central peak is heavily degraded and superimposed by an impact crater, leading to larger errors. The current crater depth cannot be used to calculate the original crater diameter because the original crater is significantly filled, making measurements of the original crater depth impossible.

5.3. Formation and Origin of Phyllosilicates

Spectral evidence for phyllosilicates (Figure 14b) within the smooth fill materials (Hfs) and dark mantling materials (Amd) point to the presence of liquid water on the surface or at depth in the past (Poulet et al., 2005; Sun & Milliken, 2015). Iron-magnesium phyllosilicates may have formed in depth by hydrothermal groundwater circulation (Ehlmann et al., 2011; Fairén et al., 2010; Schwenzer & Kring, 2009). Impacts into the Noachian plateau potentially generated hydrothermal systems in which warm groundwater circulated and altered rocks (Fairén et al., 2010; Schwenzer & Kring, 2009). According to Schwenzer and Kring (2009), the formed hydrous minerals concentrated along fractures and permeable crater portions (e.g., the central peak). Our observation of phyllosilicate distribution near the central peak of the studied cavus (Figure 14b) supports phyllosilicate formation by impact-triggered hydrothermalism. The initial cavi-forming impact induced subsurface alteration and the formation of phyllosilicates, which were excavated and redistributed by subsequent impacts. Alternatively, the phyllosilicates might have formed by aqueous alteration of volcanic ash in marine or lacustrine environments (McKeown et al., 2009). Furthermore, McKeown et al. (2009) observed that the Al-rich phyllosilicates overlay the Fe-Mg phyllosilicates in Mawrth Vallis. In our study area, we cannot observe such a relationship, but note that Al-rich phyllosilicates are less distributed (Figure 14b) and thus, might differ either in age or in origin from the Fe-Mg phyllosilicates. Dehouck et al. (2010) proposed a Hesperian deposition/formation age for hydrated minerals in the nearby Ismenius Cavus, which is consistent with our derived ages of the phyllosilicate-bearing units (Hfs), and the absence of sulfates, which were formed in more acidic environments (Poulet et al., 2005). However, we can almost certainly exclude the possibility of authigenic clay formation in the Amazonian period (Sun & Milliken, 2015) due to the alteration of the dark mantling unit (Amd) as the phyllosilicates are heterogeneously distributed and affect other geological units as well (e.g., Hfs).

Consequently, we suggest that most of the phyllosilicates in Deuteronilus Cavus were possibly formed in impact-generated hydrothermal systems in the Noachian and were redistributed by impacts (e.g., Fairén et al., 2010; Schwenzer & Kring, 2009). The surficial aqueous activity may have formed the Al-rich phyllosilicates (e.g., McKeown et al., 2009) in the Hesperian. However, detailed studies (e.g., by future landing missions) are necessary to examine whether the phyllosilicates in the Martian fretted terrain are primary materials associated with the surficial aqueous activity, subsurface alteration products excavated by impacts, or a combination of both.

6. Chronological Geological History of the Deuteronilus Cavus Region in Ismenius Lacus

On the basis of our detailed geological mapping, we interpret the geological history as follows:

1. *Ancient Basement*: We concur with McGill (2000) concerning the existence of the generally now-buried pre-Noachian heavily cratered crustal terrain, now protruding as kipukas and rims of ancient large impact craters in the region just outside our map area. This substrate is likely to be a relatively porous megaregolith composed of interleaved and admixed crater and basin ejecta deposits (McGill, 2000).
2. *Origin of Regional Plains*: We find strong evidence for the volcanic origin of the plateau unit (Nps) on the basis of (a) the flat-lying dark marker bed in valley/cavi wall outcrops in the area, lying below ∼180–300 m of less coherent and brighter material (Figure 6), (b) the subdued and regionally flat topography of the plateau (Nps), (c) the subdued wrinkle ridges occurring on the flat plateau surface of unit Nps, and (d) the paucity of buried craters protruding through the plateau surface (Nps) with diameters less than ∼30 km.
3. *Origin of the Deuteronilus Cavus*: We propose that Deuteronilus Cavus in the central map area is originally of impact origin, on the basis of (a) its generally circular shape, (b) evidence for crater wall and rim erosion and retreat (Figure 15), (c) the presence of a prominent mound centrally located in the cavi, and interpreted as a remnant central peak, and (d) the abundance of other large impact craters that experience a similar modification process (e.g., the crater to the northwest). We suggest that the cavi-forming impact occurred in the Noachian period, although the exact timing is challenging to reconstruct due to severe subsequent modification of the initial crater.
4. *Modification of Deuteronilus Cavus*: We interpret Deuteronilus Cavus to have been heavily modified during several stages of evolution: (a) on the basis of its current depth and prominence of the central peak-like structure, we interpret the crater to have been relatively fresh at the time of emplacement of the regional plains; (b) the emplacement of regional volcanic plains (to an average depth of ∼180–300 m on the basis of the paucity of remnant flooded craters below 10 km) appears to have been predominantly outside the cavi crater rim, with little evidence of volcanic resurfacing in its interior; this is consistent with other evidence for its apparent freshness, as the elevated raised rim crest would provide barriers to regional volcanic plains entering the crater and flooding the crater floor as seen in other craters in the larger region (McGill, 2000); (c) topographic cross-sections reveal no remnant of an upraised rim at the Deuteronilus Cavus rim, and the rim topography actually slopes toward the cavus interior within about 3 km of the edge of the wall; and (d) the interior wall of Deuteronilus Cavus shows convincing evidence for having been modified and backwasted by debris-covered glaciers in a zone ranging in width from ∼5 to 20 km over the majority of the cavus wall circumference. Taken together, these observations suggest a potential enlargement of the original crater of up to about 175–200 percent.
5. *Origin of the Fretted Terrain*: Key elements of the fretted terrain (stubby branching alcoves, sinuous channels, and mesas/hills (Nk) with associated LDA of unit Ada_1) occur in the mapped area and provide important evidence for the origin of the fretting process; we concur with McGill (2000) that the timing of these post-dates the regional volcanic plains. Stubby branching alcoves occur on the rims of the two 40–50 km diameter plains-embayed craters on the western map margin and in several local areas along the rim of Deuteronilus Cavus. These features range from 5 to 10 km in length to up to ∼40 km along the southern rim. Most consist of multiple stubby branches that open into the alcoves, which in turn open into the crater or cavus.
   Some stubby branching channels also transition into sinuous channels (the two located on the Deuteronilus Cavus rim to south and southwest directions). The sinuous nature of these channel segments and channels strongly supports an origin related to the flow of liquid water, but debate centers on whether the water source is related to (a) overland flow and amplified erosion at steep scarps (Lamb et al., 2006, 2007; Lapotre & Lamb, 2018) or (b) subsurface water flow and sapping-related processes (e.g., Howard et al., 1988). Erosion

by overland flow of liquid water (e.g., Lamb et al., 2006, 2007) that carves the channels at steep cliffs and slopes is an option supported in the mapped area by the presence of some associated "valley networks" in the vicinity of the stubby channels. However, these "valley networks" differ from those in the highlands in several important ways.

Contrary, the apparent emergence from below the volcanic plains surface and incision into the plains at crater and cavi rims suggests that the water may have been derived from the pre-volcanic plains highland substrate, either ground ice melted by the heat of the overlying lava or liberated groundwater (e.g., Carruthers & McGill, 1998; McGill, 2000), or associated with direct lava flow heating and melting of surface snow and ice, as seen in Hesperia Planum and elsewhere (e.g., Cassanelli & Head, 2016, 2018).

If either of the interpretations are correct, then Deuteronilus Cavus may once have had liquid water ponding on the surface, and this could potentially cause alteration of surface rocks to produce phyllosilicates. We note that the breach in the Deuteronilus Cavus wall at Mamers Valles is the same location at which Mamers displays a significant increase in its width (from 5 to 25 km) and depth, potentially signaling the drainage of water from within the cavus and the erosional widening and deepening of Mamers from this point downslope to the north.

6. *Origin of the Valley Networks*: We note that the branching fluvial channels in our study area are spatially associated with alcoves and crater/valley walls, and appear not to be related to the Late Noachian—Early Hesperian valley network systems mapped by Hynek et al. (2010) and dated by Fassett and Head (2011). Instead, they appear to be more recent based on their morphology and well-defined channel walls/floors. In addition, they are superimposed on the volcanic plains and upper mantle unit, and thus are of a different age and origin than the traditional valley networks and fretted terrain. Furthermore, they are very locally distributed and do not show evidence of regional overland flow (as in Davis et al. (2019)). They could be either linked to sapping or related to stubby channels, or, more favorably, to the glacial phase of the fretted terrain resurfacing perhaps by small amounts of melting in the waning period of a high-obliquity glaciation phase in the mid-latitudes. The latter process is consistent with our interpretation of the lobate and lineated deposits in the cavus wall circumference and valleys.
7. *Nature and Evolution of Lobate and Lineated Deposits*: The LDAs and LVF located in the cavi and fretted channels, such as Mamers Valles, are clearly separated in time from the formation of the fretted terrain and are related to Amazonian glacial modification of cavi and valley walls and massif margins (LDAs at massifs and coalesced LDAs in valley and cavi walls, and coalesced valley wall LDAs turning downslope to create LVF). The source of the glacial ice is the mid-latitude plateau glaciation (Fastook & Head, 2014; Head et al., 2005) with the ice descending down the valley and cavi walls, and the receding at the end of the glacial period to leave the debris-covered remnants we see today. Topography data suggest that LDAs in the cavi may be up to 400–600 m thick (Figure 3), consisting of several hundred meters of relatively pure ice preserved for millions of years (Helbert et al., 2005; Marchant et al., 2002) underlying the 15–20 m thick protective insulating regolith surface layer. Where the protective regolith layer was too thin, the buried ice sublimated and formed pits with polygonal fractures (AHp; Figures 8c and 8d). Furthermore, debris was not only transported by the retreating glaciers into the cavi and valleys but also deposited on the plateau (see below).
8. *Origin of the Regional Plains Light Surface Layer*: This light surface layer is superimposed on the ∼50 m thick volcanic marker bed and varies in thickness from 180 to 200 m in an outcrop on the western cavi wall to 260–300 m in Mamers Valles (Figure 6). The dark protruding layer appears to be the exposed volcanic plains. Candidate origins for the light surface layer include (a) fluvial flood plain from valley networks debouching into the Arabia terra plain (e.g., Davis et al., 2019), (b) impact ejecta, (c) volcanic tephra airfall (Kerber et al., 2012), (d) dust storm airfall, and (e) sublimation residue from dust associated with regional plateau glaciation snowfall (see Madeleine et al., 2009). The fluvial flood plain origin can be excluded due to the lack of evidence for regional overland flow and the very locally distributed branched fluvial channels. Impact ejecta up to 300 m thick over an extensive area seems unlikely, but may locally contribute to the light surface layer. In addition, volcanic tephra and dust storm airfall are not expected to form such voluminous ash accumulations in the Arabia Terra region (Kerber et al., 2012). Consequently, the preferred origin that fits the observations and can explain the majority of the several hundred meters thick light surface layer is a sublimation residue associated with Amazonian plateau glaciation snowfall (Madeleine et al., 2009). The mid-latitude plateau glaciation, with several glacial phases in which the ice descended down the valley and cavi walls and receded at the end of the glacial period, left behind debris, sublimation till, and dust. These materials formed the regional plains light surface layer and locally incorporated impact ejecta. An additional critical observation supporting the sublimation residue origin is the occurrence of pedestal (Figure 5b) and

lobate ejecta craters (Figure 5d) on the plateau, which is evidence for the presence of snow and ice when these craters formed (Fastook & Head, 2014; Weiss & Head, 2015).

7. Importance for Future Landing Missions

Our map represents the first high-resolution geological study of Deuteronilus Cavus near the enigmatic Mars dichotomy boundary. Due to the presence of ice deposits and evidence for hydrated minerals, the potential of preservation of organic matter or potential biological signatures is high (Mangold et al., 2021). Furthermore, ice deposits should be considered for future landing missions as they can be studied for climatological history and parameters, for evidence of biomarkers, and for ISRU (Plaut et al., 2009). In addition, the crater-like Deuteronilus Cavus depression contains a complex and diverse geology, which possibly enables studies of (a) at least two episodes of emplacement of ice-rich, viscous flow materials (Ada_1 and Ada_2) and older, strongly degraded apron materials (Hfc), (b) variable mineralogy of surface materials (e.g., phyllosilicates and dark, low relative brightness mantling materials (Amd)) and their origin, (c) Hesperian deposits of different morphologies and texture, which are all accessible at the surface, and (d) remnants of Noachian plateau materials located within Deuteronilus Cavus, and possibly (e) the nature of the fretted terrain and its associated processes. Thus, our research area is suitable for examinations of aeolian, fluvial, and (peri-)glacial processes as well as Amazonian, Hesperian, and Noachian materials to constrain the geologic and hydrologic evolution, and climate conditions, especially throughout the Hesperian and Amazonian periods. In addition, landing and sample-return missions would permit verification of the chronological geological history of our study area (Section 6) and address open and still puzzling morphologies and processes, such as the relationship between traditional valley networks, our branching fluvial channels and fretted channels. Of particular scientific interest is the question of whether the cavus is of impact origin, how much rim and wall retreat has occurred, and whether liquid water once ponded on the surface of the cavus and led to the alteration of rocks and the formation of phyllosilicates. In addition, voluminous ice deposits up to 600 m thick, buried at shallow depths of less than 20 m below the sublimation till, facilitate studies of the origin of the glacial ice, its potential for preserving ancient biological and climatological signatures, the scenario of an Amazonian mid-latitude plateau glaciation and its phases, and simultaneously serve as a resource for mission technical requirements.

8. Conclusion

Our map provides the first high-resolution study of Deuteronilus Cavus (~120 km diameter) in the Ismenius Lacus region centered at 36.2°N and 14.0°E. The ancient basement substrate is likely a relatively porous megaregolith composed of interleaved and mixed crater and basin ejecta deposits (McGill, 2000). We find strong evidence for the volcanic origin of the regional plateau (Nps) based on the ~50 m thick, volcanic, dark marker bed in valley walls that lie beneath 180–300 m of less coherent and brighter material. Furthermore, we propose that pervasive external volcanic flooding and internal erosional modification and enlargement of a pre-existing crater by backwasting, top-down melting of snow/ice, and widening of tributary valleys resulted in the present shape of Deuteronilus Cavus and the absence of characteristic features such as any discernible rim topography. Taken together, these observations suggest a possible enlargement of the original crater by up to 175%–200%. The timing of the formation of the fretted terrain and Mamers Valles postdates the regional volcanic plains. The fretted terrain formation due to flowing water led to ponded water on the surface of the cavus, forming channels (now observed as inverted sinuous ridges) and potentially causing alteration of surface rocks. The phyllosilicates detected in the smooth fill materials (Hfs) and the dark mantling unit (Amd) could be primary materials associated with the surficial aqueous activity, subsurface alteration products excavated by impacts, or a combination of both. We note that the breach in the cavus wall at Mamers Valles is the same location where Mamers shows a significant increase in width (from 5 to 25 km) and depth, possibly signaling the drainage of water from Deuteronilus Cavus and the erosional widening and deepening of Mamers from this point downslope to the north. However, the branching fluvial channels differ from the traditional Late Noachian—Early Hesperian valley networks. Instead, they appear to be more recent, are spatially related to alcoves, and they could be either linked to sapping and related to stubby channels, or to the glacial phase of the fretted terrain resurfacing perhaps by small amounts of melting in the waning period of a high-obliquity glaciation phase in the mid-latitudes. The latter candidate origin is consistent with our interpretation of the lobate and lineated deposits in the cavus wall circumference and valleys. These deposits can be up to 600 m thick, are clearly separated in time from the formation of

the fretted terrain and are related to Amazonian glacial modification of the cavi/valley walls and massif margins. The receding glaciers at the end of the last glacial period left behind the debris-covered LDAs and LVF. Several hundred meters of relatively pure ice incorporated in the remnants and protected by a 15–20 m insulating debris layer are of outstanding interest for future landing missions because of their potential to preserve biological and climatological signatures, to provide a critical test of the high-obliquity mid-latitude Amazonian plateau glaciation, and to be used for ISRU. Taken together, the geologic inventory of our study area reveals deposits formed by fluvial, (peri-)glacial, and aeolian processes throughout Martian history, spanning Noachian, Hesperian, and Amazonian times. Further studies of the Arabia Terra— DM region can help to address outstanding scientific questions, such as the relationships between the branching fluvial channels of our map, the traditional valley networks, and the fundamental origin of the fretted terrain and its associated processes in space and time, in a regional and thus more representative context.

Appendix A

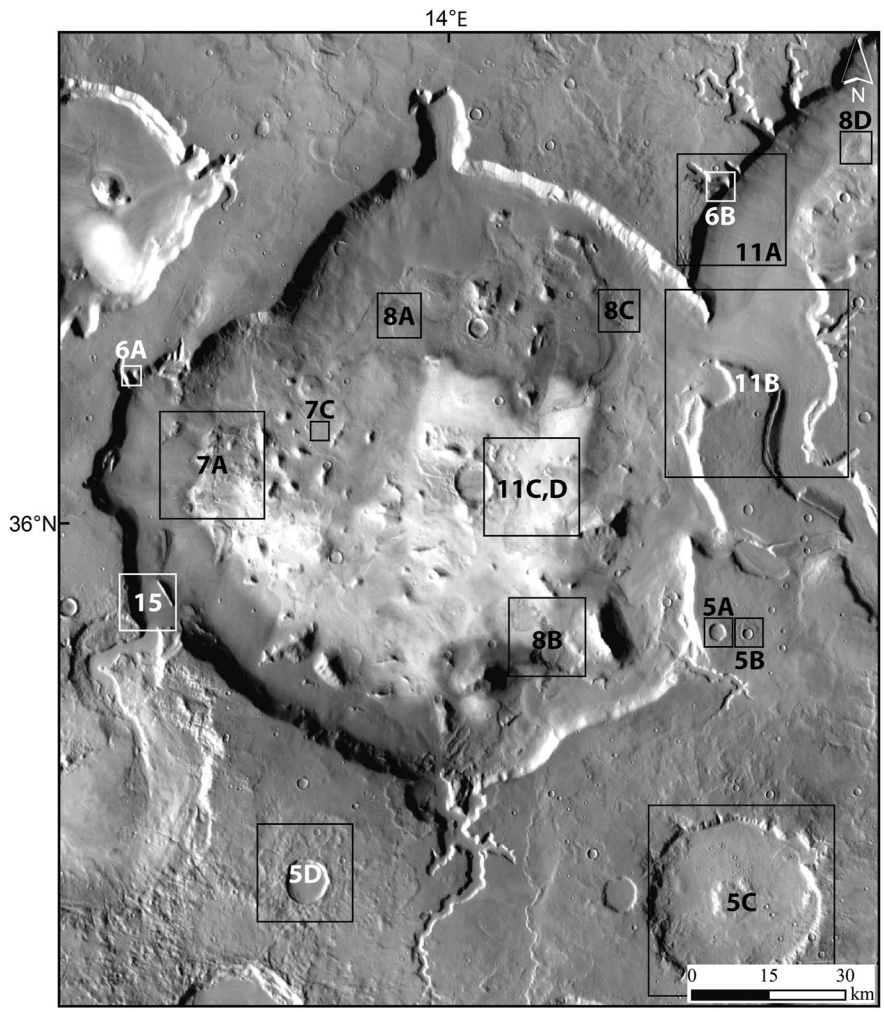

Figure A1. Reference map showing the location of the figures in our survey area on a THEMIS-IR daytime basemap. The locations of figures showing surface textures or small craters are not shown due to their limited extent, but their HiRISE image IDs are given in the figure captions.

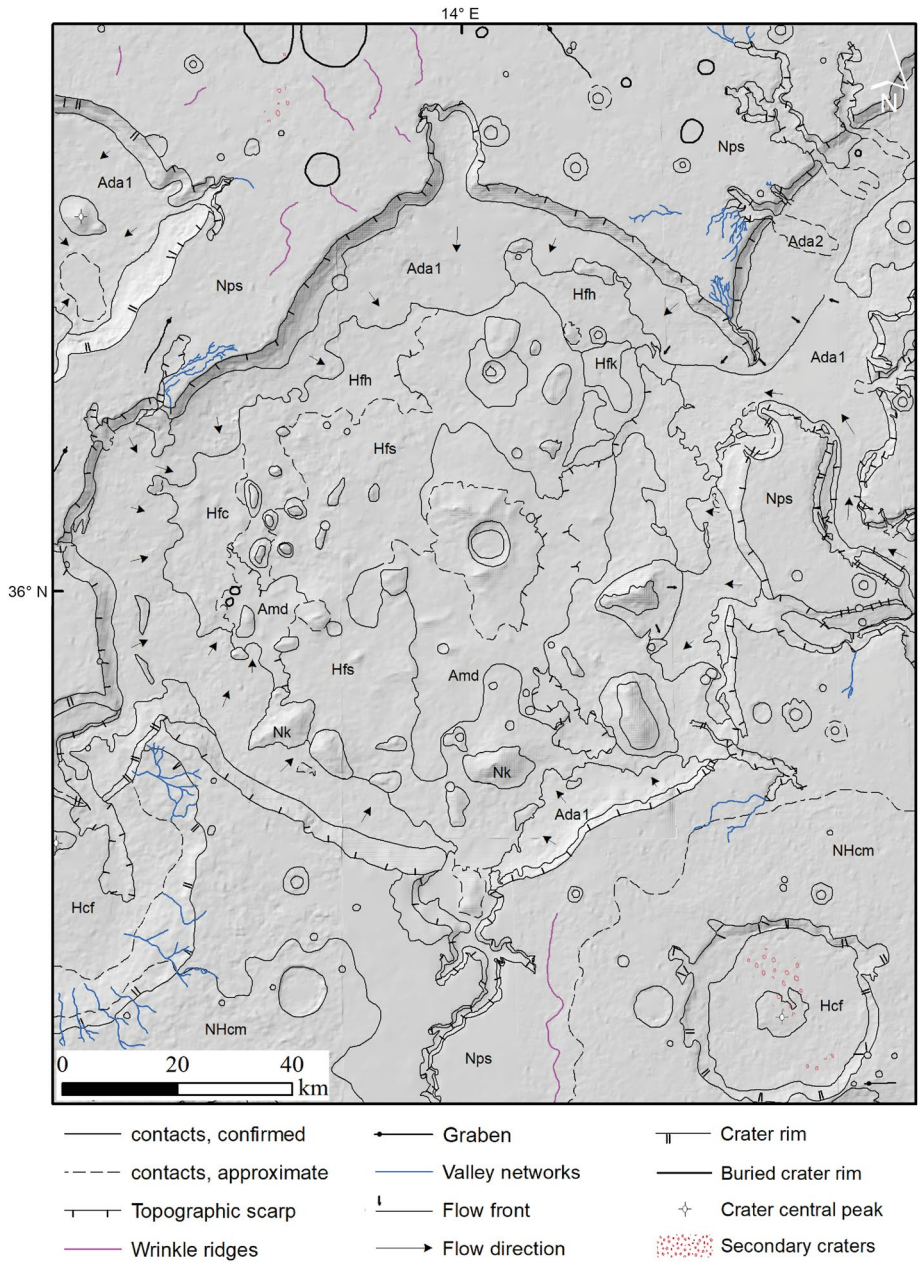

Figure A2. Geological map without unit colors to emphasize the linear features, their distribution, and their relationships with a HRSC-DTM hillshade basemap.

Conflict of Interest

The authors declare no conflicts of interest relevant to this study.

Data Availability Statement

The final geologic map product is available via Zenodo (Wueller et al., 2023): https://doi.org/10.5281/zenodo.8205276.

THEMIS-IR data are available from the PDS (Christensen, 2002). CTX data are available from the PDS (Malin, 2007). HiRISE images are available from the PDS (McEwen, 2007). HRSC data are available from ESA (European Space Agency, 2020).

Acknowledgments
H.H. and W.I. are supported by the German Aerospace Center (Deutsches Zentrum für Luft- und Raumfahrt) Project 50OO2102. J.W.H. is a visiting professor at the Institut für Planetologie, Universität Münster. In addition, we would like to thank the HRSC instrument team for the successful planning and acquisition of the data. We further appreciate fruitful discussions and comments from Lennard Pauw (Institute of Planetology, Universität Münster) during the initial phase of mapping and writing. Finally, we wish to thank Sarah Black and an anonymous reviewer for their thoughtful and thorough comments, which greatly improved our publication. Open Access funding enabled and organized by Projekt DEAL.

References

Andrews-Hanna, J. C., Zuber, M. T., & Banerdt, W. B. (2008). The Borealis basin and the origin of the martian crustal dichotomy. *Nature*, *453*(7199), 1212–1215. https://doi.org/10.1038/nature07011

Baker, D. M. H., & Head, J. W. (2015). Extensive Middle Amazonian mantling of debris aprons and plains in Deuteronilus Mensae, Mars: Implications for the record of mid-latitude glaciation. *Icarus*, *260*, 269–288. https://doi.org/10.1016/j.icarus.2015.06.036

Batson, R. M., Bridges, P. M., & Inge, J. L. (1979). *Atlas of Mars: The 1: 5,000,000 map series* (Vol. 438). NASA, USGS.

Blue, J. (1999). *Gazetteer of planetary nomenclature*. USGS.

Carr, M. H. (2006). *The surface of Mars*. Cambridge University Press.

Carr, M. H. (1995). The Martian drainage system and the origin of valley networks and fretted channels. *Journal of Geophysical Research*, *100*(E4), 7479–7507. https://doi.org/10.1029/95je00260

Carr, M. H., & Head, J. W. (2010). Geologic history of Mars. *Earth and Planetary Science Letters*, *294*(3–4), 185–203. https://doi.org/10.1016/j.epsl.2009.06.042

Carruthers, M. W., & McGill, G. E. (1998). Evidence for igneous activity and implications for the origin of a fretted channel in southern Ismenius Lacus, Mars. *Journal of Geophysical Research*, *103*(E13), 31433–31443. https://doi.org/10.1029/98je02494

Cassanelli, J. P., & Head, J. W. (2016). Lava heating and loading of ice sheets on early Mars: Predictions for meltwater generation, groundwater recharge, and resulting landforms. *Icarus*, *271*, 237–264. https://doi.org/10.1016/j.icarus.2016.02.004

Cassanelli, J. P., & Head, J. W. (2018). Formation of outflow channels on Mars: Testing the origin of Reull Vallis in Hesperia Planum by large-scale lava-ice interactions and top-down melting. *Icarus*, *305*, 56–79. https://doi.org/10.1016/j.icarus.2018.01.001

Christensen, P. R. (2002). Odyssey THEMIS ir RDR V1.0 [Dataset]. NASA Planetary Data System. https://doi.org/10.17189/1520332

Christensen, P. R., Jakosky, B. M., Kieffer, H. H., Malin, M. C., Mcsween, H. Y., Nealson, K., et al. (2004). The thermal emission imaging system (THEMIS) for the Mars 2001 Odyssey mission. *Space Science Reviews*, *110*(1/2), 85–130. https://doi.org/10.1023/b:spac.0000021008.16305.94

Chuang, F. C., & Crown, D. A. (2009). Geologic map of MTM 35337, 40337 and 45337 quadrangles, Deuteronilus Mensae region of Mars: U.S. Geological Survey Scientific Investigation Map 3079, pamphlet 17 (p. 1). Retrieved from http://pubs.usgs.gov/sim/3079

Craddock, R. A., & Howard, A. D. (2002). The case for rainfall on a warm, wet early Mars. *Journal of Geophysical Research*, *107*(11), 21-1–21-36. https://doi.org/10.1029/2001JE001505

Croft, S. K. (1981). Hypervelocity impact craters in icy media. *Lunar and Planetary Science XII*, *12*, 190–192.

Davis, J. M., Gupta, S., Balme, M., Grindrod, P. M., Fawdon, P., Dickeson, Z. I., & Williams, R. M. E. (2019). A diverse array of fluvial depositional systems in Arabia Terra: Evidence for mid-Noachian to early Hesperian rivers on Mars. *Journal of Geophysical Research: Planets*, *124*(7), 1913–1934. https://doi.org/10.1029/2019je005976

Dehouck, E., Mangold, N., le Mouélic, S., Ansan, V., & Poulet, F. (2010). Ismenius Cavus, Mars: A deep paleolake with phyllosilicate deposits. *Planetary and Space Science*, *58*(6), 941–946. https://doi.org/10.1016/j.pss.2010.02.005

Dickson, J. L., Kerber, L. A., Fassett, C. I., & Ehlmann, B. L. (2018). A global, blended CTX mosaic of Mars with vectorized seam mapping: A new mosaicking pipeline using principles of non-destructive image editing. In *Lunar and planetary science conference* (Vol. 49, pp. 1–2). Lunar and Planetary Institute The Woodlands TX.

Ehlmann, B. L., Mustard, J. F., Murchie, S. L., Bibring, J.-P., Meunier, A., Fraeman, A. A., & Langevin, Y. (2011). Subsurface water and clay mineral formation during the early history of Mars. *Nature*, *479*(7371), 53–60. https://doi.org/10.1038/nature10582

European Space Agency. (2020). MEX-M-HRSC-5-REFDR-MAPPROJECTED [Dataset]. MEX-M-HRSC-5-REFDR-MAPPROJECTED. European Space Agency. https://doi.org/10.5270/esa-pm8ptbq

Fairén, A. G., Chevrier, V., Abramov, O., Marzo, G. A., Gavin, P., Davilla, A. F., et al. (2010). Noachian and more recent phyllosilicates in impact craters on Mars. *Proceedings of the National Academy of Sciences of the United States of America*, *107*(27), 12095–12100. https://doi.org/10.1073/pnas.1002889107

Fassett, C. I., & Head, J. W. (2011). Sequence and timing of conditions on early Mars. *Icarus*, *211*(2), 1204–1214. https://doi.org/10.1016/j.icarus.2010.11.014

Fastook, J. L., & Head, J. W. (2014). Amazonian mid- to high-latitude glaciation on Mars: Supply-limited ice sources, ice accumulation patterns, and concentric crater fill glacial flow and ice sequestration. *Planetary and Space Science*, *91*, 60–76. https://doi.org/10.1016/j.pss.2013.12.002

Fastook, J. L., & Head, J. W. (2015). Glaciation in the Late Noachian Icy Highlands: Ice accumulation, distribution, flow rates, basal melting, and top-down melting rates and patterns. *Planetary and Space Science*, *106*, 82–98. https://doi.org/10.1016/j.pss.2014.11.028

Fastook, J. L., Head, J. W., & Marchant, D. R. (2014). Formation of lobate debris aprons on Mars: Assessment of regional ice sheet collapse and debris-cover armoring. *Icarus*, *228*, 54–63. https://doi.org/10.1016/j.icarus.2013.09.025

Federal Geographic Data Committee. (2006). 25-Planetary geology features, Pub. L. No. FGDC-STD-013-2016, FGDC STD 013-2016, appendix A, FGDC digital geographic standard for geologic map symbolization. Retrieved from https://ngmdb.usgs.gov/fgdc_gds/geolsymstd.php

Fergason, R. L., & Christensen, P. R. (2008). Formation and erosion of layered materials: Geologic and dust cycle history of eastern Arabia Terra, Mars. *Journal of Geophysical Research*, *113*(E12), E12001. https://doi.org/10.1029/2007je002973

Fergason, R. L., Hare, T. M., & Laura, J. (2018). *HRSC and MOLA blended digital elevation model at 200m v2. Astrogeology PDS annex*. U.S. Geological Survey. Retrieved from http://bit.ly/HRSC_MOLA_Blend_v0

Garvin, J. B., Sakimoto, S. E. H., & Frawley, J. J. (2003). Craters on Mars: Global geometric properties from gridded MOLA topography. In *Sixth international conference on Mars*. Lunar and Planetary Institute.

Grau Galofre, A., Jellinek, A. M., & Osinski, G. R. (2020). Valley formation on early Mars by subglacial and fluvial erosion. *Nature Geoscience*, *13*(10), 663–668. https://doi.org/10.1038/s41561-020-0618-x

Greeley, R., & Guest, J. E. (1987). Geologic map of the eastern equatorial region of Mars: U.S. Investigations map 1802-B, 1 plate. https://doi.org/10.3133/i1802B

Hamlin, S. E., Kargel, J. S., Tanaka, K. L., Lewis, K. J., & Macayeal, D. R. (2000). Preliminary studies of icy debris flows in the martian fretted terrain. In *Lunar and Planetary Science Conference* (Vol. 31, p. 1785).

Hartmann, W. K. (2005). Martian cratering 8: Isochron refinement and the chronology of Mars. *Icarus*, *174*(2 SPEC. ISS.), 294–320. https://doi.org/10.1016/j.icarus.2004.11.023

Head, J. W., Marchant, D. R., Agnew, M. C., Fassett, C. I., & Kreslavsky, M. A. (2006). Extensive valley glacier deposits in the northern mid-latitudes of Mars: Evidence for Late Amazonian obliquity-driven climate change. *Earth and Planetary Science Letters*, *241*(3–4), 663–671. https://doi.org/10.1016/j.epsl.2005.11.016

Head, J. W., Mustard, J. F., Kreslavsky, M. A., Milliken, R. E., & Marchant, D. R. (2003). Recent ice ages on Mars. *Nature*, *426*(6968), 797–802. https://doi.org/10.1038/nature02114

Head, J. W., Neukum, G., Jaumann, R., Hiesinger, H., Hauber, E., Carr, M., et al. (2005). Tropical to mid-latitude snow and ice accumulation, flow and glaciation on Mars. *Nature*, *434*(7031), 346–351. https://doi.org/10.1038/nature03359
Head, J. W., III, Kreslavsky, M. A., & Pratt, S. (2002). Northern lowlands of Mars: Evidence for widespread volcanic flooding and tectonic deformation in the Hesperian period. *Journal of Geophysical Research*, *107*(E1), 1–3. https://doi.org/10.1029/2000je001445
Helbert, J., Reiss, D., Hauber, E., & Benkhoff, J. (2005). Limits on the burial depth of glacial ice deposits on the flanks of Hecates Tholus, Mars. *Geophysical Research Letters*, *32*(17), L17201. https://doi.org/10.1029/2005gl023712
Heyer, T., Hiesinger, H., Erkeling, G., Bernhardt, H., Luesebrink, D., & Jaumann, R. (2018). The multi-temporal Database of planetary image data (MUTED): A web-based tool for studying dynamic Mars. *Planetary and Space Science*, *159*, 56–65. https://doi.org/10.1016/j.pss.2018.04.015
Hiesinger, H., & Tanaka, K. (2020). The planetary time scale. In *Geologic time scale 2020* (pp. 443–480). Elsevier. https://doi.org/10.1016/B978-0-12-824360-2.00015-2
Howard, A. D., Kochel, R. C., & Holt, H. E. (1988). *Sapping features of the Colorado Plateau: A comparative planetary geology field guide* (Vol. 491). Scientific and Technical Information Office, National Aeronautics and Space Administration.
Hynek, B. M., Beach, M., & Hoke, M. R. T. (2010). Updated global map of Martian valley networks and implications for climate and hydrologic processes. *Journal of Geophysical Research*, *115*(E9), E09008. https://doi.org/10.1029/2009je003548
Ivanov, B. A. (2001). Mars/Moon cratering rate ratio estimates. *Chronology and Evolution of Mars*, *96*, 87–104.
Jawin, E. R., & Head, J. W. (2021). Patterns of late Amazonian deglaciation from the distribution of martian paraglacial features. *Icarus*, *355*, 114117. https://doi.org/10.1016/j.icarus.2020.114117
Jawin, E. R., Head, J. W., & Marchant, D. R. (2018). Transient post-glacial processes on Mars: Geomorphologic evidence for a paraglacial period. *Icarus*, *309*, 187–206. https://doi.org/10.1016/j.icarus.2018.01.026
Kato, M., Iijima, Y.-I., Arakawa, M., Okimura, Y., Fujimura, A., Maeno, N., & Mizutani, H. (1995). Ice-on-ice impact experiments. *Icarus*, *113*(2), 423–441. https://doi.org/10.1006/icar.1995.1032
Kerber, L., Head, J. W., Madeleine, J.-B., Forget, F., & Wilson, L. (2012). The dispersal of pyroclasts from ancient explosive volcanoes on Mars: Implications for the friable layered deposits. *Icarus*, *219*(1), 358–381. https://doi.org/10.1016/j.icarus.2012.03.016
Kite, E. S., Michaels, T. I., Rafkin, S., Manga, M., & Dietrich, W. E. (2011). Localized precipitation and runoff on Mars. *Journal of Geophysical Research*, *116*(7), E07002. https://doi.org/10.1029/2010JE003783
Kress, A. M., & Head, J. W. (2008). Ring-mold craters in lineated valley fill and lobate debris aprons on Mars: Evidence for subsurface glacial ice. *Geophysical Research Letters*, *35*(23), L23206. https://doi.org/10.1029/2008gl035501
Lamb, M. P., Howard, A. D., Dietrich, W. E., & Perron, J. T. (2007). Formation of amphitheater-headed valleys by waterfall erosion after large-scale slumping on Hawai'i. *Geological Society of America Bulletin*, *119*(7–8), 805–822. https://doi.org/10.1130/b25986.1
Lamb, M. P., Howard, A. D., Johnson, J., Whipple, K. X., Dietrich, W. E., & Perron, J. T. (2006). Can springs cut canyons into rock? *Journal of Geophysical Research*, *111*(7), E07002. https://doi.org/10.1029/2005JE002663
Lapotre, M. G. A., & Lamb, M. P. (2018). Substrate controls on valley formation by groundwater on Earth and Mars. *Geology*, *46*(6), 531–534. https://doi.org/10.1130/g40007.1
Levy, J. S., Head, J. W., & Marchant, D. R. (2009). Concentric crater fill in Utopia Planitia: History and interaction between glacial "brain terrain" and periglacial mantle processes. *Icarus*, *202*(2), 462–476. https://doi.org/10.1016/j.icarus.2009.02.018
Lucchitta, B. K. (1977). Geology of the Ismenius Lacus quadrangle (MC-5), Mars. *NASA Technical Memorandum*, *3511*, 215–216.
Lucchitta, B. K. (1978). Geologic map of the Ismenius Lacus quadrangle of Mars: U.S. Geological survey investigations map 1065. https://doi.org/10.3133/i1065
Lucchitta, B. K. (1984). Ice and debris in the fretted terrain, Mars. *Journal of Geophysical Research*, *89*(S02), 409–418. https://doi.org/10.1029/jb089is02p0b409
Madeleine, J. B., Forget, F., Head, J. W., Levrard, B., Montmessin, F., & Millour, E. (2009). Amazonian northern mid-latitude glaciation on Mars: A proposed climate scenario. *Icarus*, *203*(2), 390–405. https://doi.org/10.1016/j.icarus.2009.04.037
Malin, M. C. (2007). MRO Context Camera experiment data record level 0 v1.0 [Dataset]. NASA Planetary Data System. https://doi.org/10.17189/1520266
Mangold, N. (2003). Geomorphic analysis of lobate debris aprons on Mars at Mars Orbiter Camera scale: Evidence for ice sublimation initiated by fractures. *Journal of Geophysical Research*, *108*(4), 8021. https://doi.org/10.1029/2002je001885
Mangold, N. (2011). Water ice sublimation-related landforms on Mars. *Geological Society - Special Publications*, *356*(1), 133–149. https://doi.org/10.1144/SP356.8
Mangold, N., Adeli, S., Conway, S., Ansan, V., & Langlais, B. (2012). A chronology of early Mars climatic evolution from impact crater degradation. *Journal of Geophysical Research*, *117*(4), E04003. https://doi.org/10.1029/2011JE004005
Mangold, N., Allemand, P., Duval, P., Geraud, Y., & Thomas, P. (2002). Experimental and theoretical deformation of ice-rock mixtures: Implications on rheology and ice content of Martian permafrost. *Planetary and Space Science*, *50*(4), 385–401. https://doi.org/10.1016/s0032-0633(02)00005-3
Mangold, N., Gupta, S., Gasnault, O., Dromart, G., Tarnas, J. D., Sholes, S. F., et al. (2021). Perseverance rover reveals an ancient delta-lake system and flood deposits at Jezero crater, Mars. *Science*, *374*(6568), 711–717. https://doi.org/10.1126/science.abl4051
Marchant, D. R., Lewis, A. R., Phillips, W. M., Moore, E. J., Souchez, R. A., Denton, G. H., et al. (2002). Formation of patterned ground and sublimation till over Miocene glacier ice in Beacon Valley, southern Victoria Land, Antarctica. *Geological Society of America Bulletin*, *114*(6), 718–730. https://doi.org/10.1130/0016-7606(2002)114<0718:fopgas>2.0.co;2
McEwen, A. (2007). Mars reconnaissance orbiter high resolution imaging science experiment, reduced data record, MRO-M-HIRISE-3-RDR-V1.1. *NASA Planetary Data System*. https://doi.org/10.17189/1520303
McGill, G. E. (2000). Crustal history of north central Arabia terra, Mars. *Journal of Geophysical Research*, *105*(E3), 6945–6959. https://doi.org/10.1029/1999je001175
Mc Keown, L. E., Bourke, M. C., & McElwaine, J. N. (2017). Experiments on sublimating carbon dioxide ice and implications for contemporary surface processes on Mars. *Scientific Reports*, *7*(1), 14181. https://doi.org/10.1038/s41598-017-14132-2
McKeown, N. K., Bishop, J. L., Noe Dobrea, E. Z., Ehlmann, B. L., Parente, M., Mustard, J. F., et al. (2009). Characterization of phyllosilicates observed in the central Mawrth Vallis region, Mars, their potential formation process, and implications for past climate. *Journal of Geophysical Research*, *114*(E2), E00D10. https://doi.org/10.1029/2008JE003301
Michalski, J. R., & Bleacher, J. E. (2013). Supervolcanoes within an ancient volcanic province in Arabia terra, Mars. *Nature*, *502*(7469), 47–52. https://doi.org/10.1038/nature12482
Morgan, G. A., Head, J. W., & Marchant, D. R. (2009). Lineated valley fill (LVF) and lobate debris aprons (LDA) in the Deuteronilus Mensae northern dichotomy boundary region, Mars: Constraints on the extent, age and episodicity of Amazonian glacial events. *Icarus*, *202*(1), 22–38. https://doi.org/10.1016/j.icarus.2009.02.017

Morgan, G. A., Putzig, N. E., Perry, M. R., Sizemore, H. G., Bramson, A. M., Petersen, E. I., et al. (2021). Availability of subsurface water-ice resources in the northern mid-latitudes of Mars. *Nature Astronomy*, *5*(3), 230–236. https://doi.org/10.1038/s41550-020-01290-z

Neukum, G., Jaumann, R., Hoffmann, H., Hauber, E., Head, J. W., Basilevsky, A. T., et al. (2004). Recent and episodic volcanic and glacial activity on Mars revealed by the high resolution stereo Camera. *Nature*, *432*(7020), 971–979. https://doi.org/10.1038/nature03231

Noe Dobrea, E. Z., Bishop, J. L., McKeown, N. K., Fu, R., Rossi, C. M., Michalski, J. R., et al. (2010). Mineralogy and stratigraphy of phyllosilicate-bearing and dark mantling units in the greater Mawrth Vallis/west Arabia Terra area: Constraints on geological origin. *Journal of Geophysical Research*, *115*(E7), E00D19. https://doi.org/10.1029/2009JE003351

Pauw, L., Wueller, L., & Hiesinger, H. (2023). Geologic map of the Deuteronilus Mensae region: Insights into the history of Mars. *LPI Contribution*, *2806*, 2459. https://doi.org/10.5281/zenodo.8205846

Plaut, J. J., Safaeinili, A., Holt, J. W., Phillips, R. J., Head, J. W., Seu, R., et al. (2009). Radar evidence for ice in lobate debris aprons in the mid-northern latitudes of Mars. *Geophysical Research Letters*, *36*(2), L02203. https://doi.org/10.1029/2008gl036379

Poulet, F., Bibring, J. P., Mustard, J. F., Gendrin, A., Mangold, N., Langevin, Y., et al. (2005). Phyllosilicates on Mars and implications for early martian climate. *Nature*, *438*(7068), 623–627. https://doi.org/10.1038/nature04274

Schwenzer, S. P., & Kring, D. A. (2009). Impact-generated hydrothermal systems capable of forming phyllosilicates on Noachian Mars. *Geology*, *37*(12), 1091–1094. https://doi.org/10.1130/G30340A.1

Sharp, R. P. (1973). Mars: Fretted and chaotic terrains. *Journal of Geophysical Research*, *78*(20), 4073–4083. https://doi.org/10.1029/jb078i020p04073

Sun, V. Z., & Milliken, R. E. (2015). Ancient and recent clay formation on Mars as revealed from a global survey of hydrous minerals in crater central peaks. *Journal of Geophysical Research: Planets*, *120*(12), 2293–2332. https://doi.org/10.1002/2015JE004918

Tanaka, K. L., Robbins, S. J., Fortezzo, C. M., Skinner, J. A., & Hare, T. M. (2014). Geologic map of Mars: U.S. Geological survey scientific investigations map 3292, pamphlet 48p. https://doi.org/10.3133/sim3292

Tanaka, K. L., Skinner, J. A., Crumpler, L. S., & Dohm, J. M. (2009). Assessment of planetary geologic mapping techniques for Mars using terrestrial analogs: The SP Mountain area of the San Francisco Volcanic Field, Arizona. *Planetary and Space Science*, *57*(5–6), 510–532. https://doi.org/10.1016/j.pss.2008.06.012

Tanaka, K. L., Skinner, J. A., & Hare, T. M. (2005). Geologic map of the northern plains of Mars: U.S. Geological survey scientific investigation map 288, pamphlet 32p. Retrieved from https://pubs.usgs.gov/sim/2005/2888

van Gasselt, S., Hauber, E., & Neukum, G. (2010). Lineated valley fill at the Martian dichotomy boundary: Nature and history of degradation. *Journal of Geophysical Research*, *115*(8), E08003. https://doi.org/10.1029/2009JE003336

van Gasselt, S., Hauber, E., Rossi, A. P., Dumke, A., Orosei, R., & Neukum, G. (2011). Periglacial geomorphology and landscape evolution of the Tempe Terra region, Mars. *Geological Society - Special Publications*, *356*(1), 43–67. https://doi.org/10.1144/SP356.4

Weiss, D. K., & Head, J. W. (2015). Crater degradation in the Noachian highlands of Mars: Assessing the hypothesis of regional snow and ice deposits on a cold and icy early Mars. *Planetary and Space Science*, *117*, 401–420. https://doi.org/10.1016/j.pss.2015.08.009

Wueller, L., Iqbal, W., Hiesinger, H., & Head, J. (2023). Geologic history of Deuteronilus cavus in the Ismenius Lacus region, Mars. (Version 1) [Dataset]. Zenodo. https://doi.org/10.5281/zenodo.8205276